Redox Biology 57 (2022) 102470

Contents lists available at ScienceDirect

Redox Biology

journal homepage: www.elsevier.com/locate/redox

Nrf1 is an indispensable redox-determining factor for mitochondrial homeostasis by integrating multi-hierarchical regulatory networks

Shaofan Hu [a,b,c], Jing Feng [a,b,c], Meng Wang [a,c], Reziyamu Wufuer [a,b,c], Keli Liu [a,b,c], Zhengwen Zhang [d], Yiguo Zhang [b,c,*]

[a] Bioengineering College and Graduate School, Chongqing University, No. 174 Shazheng Street, Shapingba District, Chongqing, 400044, China
[b] Chongqing University Jiangjin Hospital, School of Medicine, Chongqing University, No. 725 Jiangzhou Avenue, Dingshan Street, Jiangjin District, Chongqing, 402260, China
[c] The Laboratory of Cell Biochemistry and Topogenetic Regulation, College of Bioengineering & Faculty of Medical Sciences, Chongqing University, No. 174 Shazheng Street, Shapingba District, Chongqing, 400044, China
[d] Laboratory of Neuroscience, Institute of Cognitive Neuroscience and School of Pharmacy, University College London, 29-39 Brunswick Square, London, WC1N 1AX, England, United Kingdom

ARTICLE INFO

Keywords:
Nrf1
Nrf2
αPal^{NRF1}
GABP^{NRF2}
UCP2
ROS
Redox regulation
Antioxidant response
Mitochondrion
Metabolism
UPR^{mt}
miR-195
miR-497

ABSTRACT

To defend against a vast variety of challenges in oxygenated environments, all life forms have evolutionally established a set of antioxidants, detoxification, and cytoprotective systems during natural selection and adaptive survival, to maintain cell redox homeostasis and organ integrity in the healthy development and growth. Such antioxidant defense systems are predominantly regulated by two key transcription factors Nrf1 and Nrf2, but the underlying mechanism(s) for their coordinated redox control remains elusive. Here, we found that loss of full-length Nrf1 led to a dramatic increase in reactive oxygen species (ROS) and oxidative damages in *Nrf1α*$^{-/-}$ cells, and this increase was not eliminated by drastic elevation of Nrf2, even though the antioxidant systems were also substantially enhanced by hyperactive Nrf2. Further studies revealed that the increased ROS production in *Nrf1α*$^{-/-}$ resulted from a striking impairment in the mitochondrial oxidative respiratory chain and its gene expression regulated by nuclear respiratory factors, called αPal^{NRF1} and GABP^{NRF2}. In addition to the antioxidant capacity of cells, glycolysis was greatly augmented by aberrantly-elevated Nrf2, so to partially relieve the cellular energy demands, but aggravate its mitochondrial stress. The generation of ROS was also differentially regulated by Nrf1 and Nrf2 through miR-195 and/or mIR-497-mediated UCP2 pathway. Consequently, the epithelial-mesenchymal transformation (EMT) of *Nrf1α*$^{-/-}$ cells was activated by putative ROS-stimulated signaling *via* MAPK, HIF1α, NF-kB, PI3K and AKT, all players involved in cancer development and progression. Taken together, it is inferable that Nrf1 acts as a potent integrator of redox regulation by multi-hierarchical networks.

1. Introduction

Under the oxygenated environments, almost all cellular life forms have been successively generating, transforming and eliminating those reactive oxygen species (ROS, also including reactive nitrogen and sulphur species) in a variety of cell processes (e.g., metabolism, proliferation, differentiation), immune regulation and vascular remodeling [1]. Approximately 90% of ROS in eukaryotic cells are generated from the mitochondria, which are hence accepted as a major source of intracellularly-producing ROS. Approximately 2% of oxygens are consumed by mitochondria to produce ROS, and this number could be incremented when their electron transport chains (ETCs) are damaged and/or uncoupled with oxidative phosphorylation (OXPHOS, for ATP production) [2]. Besides, NADPH oxidases, cytochrome p450 isoenzymes and the other oxidases existing particularly in the peroxisome and endoplasmic reticulum (ER) are considered as the secondary sources of ROS production [3]. ROS are endowed with a cytotoxic capability to beget oxidative damage and even lead to cell death if excessive ROS is yielded. To defend against potential challenges from oxidative stress, all life forms have also evolutionally established a set of antioxidant, detoxification and cytoprotective systems to maintain cellular redox homeostasis and organ integrity during their adaptive survival. Such a

* Corresponding author. Chongqing University Jiangjin Hospital, School of Medicine, Chongqing University, No. 725 Jiangzhou Avenue, Dingshan Street, Jiangjin District, Chongqing, 402260, China.
E-mail addresses: yiguozhang@cqu.edu.cn, eaglezhang64@gmail.com (Y. Zhang).

https://doi.org/10.1016/j.redox.2022.102470
Received 18 August 2022; Received in revised form 4 September 2022; Accepted 7 September 2022
Available online 13 September 2022

homeodynamic balance between oxidative stress and antioxidant defense system has been established and also perpetuated at a steady state of redox, just at which all living organisms are allowed for healthy survival under such robust redox homeostasis.

Collectively, the levels of ROS (albeit with higher cytotoxicity) under the normal conditions are finely tuned and also restricted to considerably lower extents, such that they can also serve as potent eustress that triggers certain hormestic effects on the physiology of living organisms insomuch as to preserve the healthy life processes [4,5]. Thereby, a redox threshold is set at a certain steady-state of physiology. Once ROS are produced to exceed the preformed redox threshold, they exert oxidative distress to stimulate a vast variety of pathophysiological responses and even pathological effects to different extents [6]. The proper ROS levels are required to induce many biological activities, including development, growth, cell division, proliferation, differentiation, survival and apoptosis, as well as immune responses [1,3]. Rather,

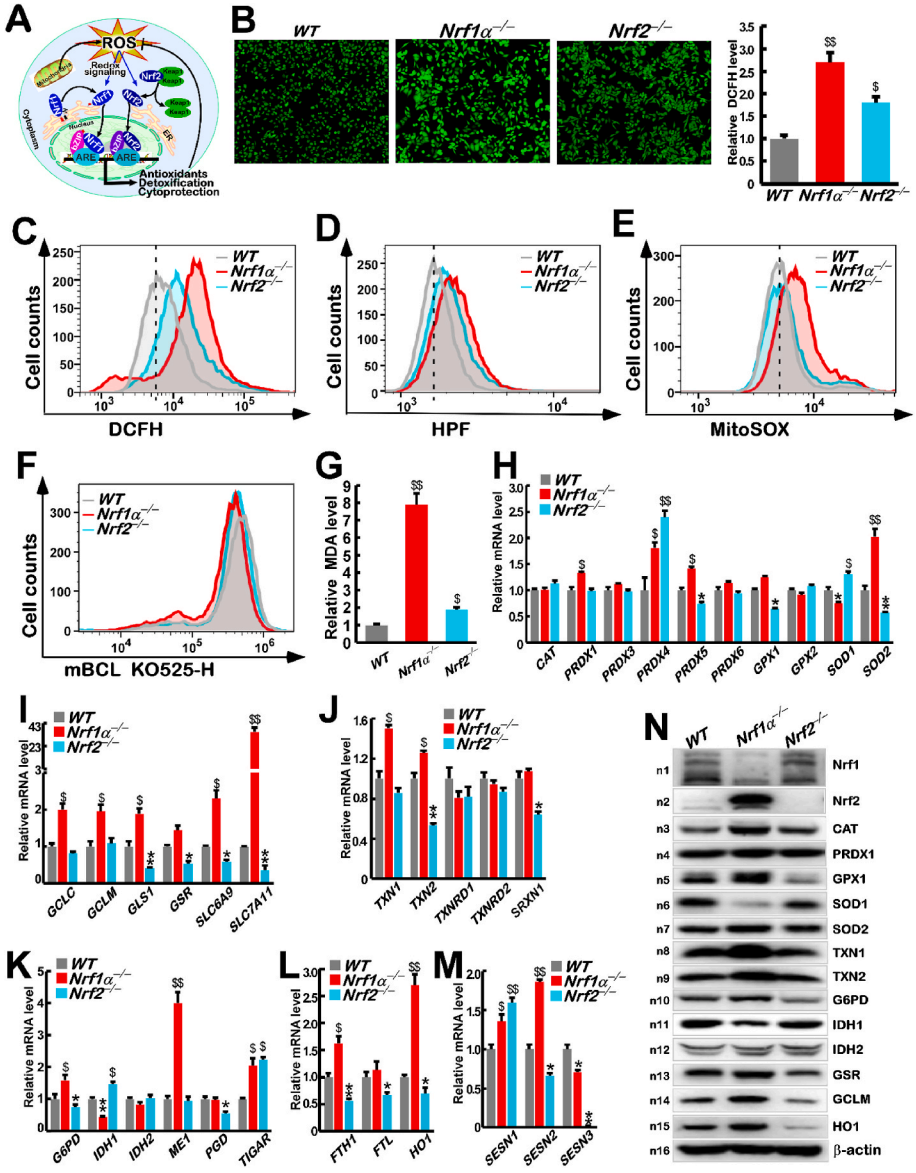

Fig. 1. Distinctions in the redox status and expression of antioxidant genes in *WT*, *Nrf1α*$^{-/-}$ and *Nrf2*$^{-/-}$ cell lines.

(A) A schematic representation of signaling mechanisms that Nrf1 and Nrf2 are activated by ROS to play cytoprotective roles.

(B) Fluorescence images representing the ROS levels in *WT*, *Nrf1α*$^{-/-}$ and *Nrf2*$^{-/-}$ cells, which were stained by DCFH-DA (excited in 488 nm). The fluorescence intensity was statistically calculated as fold changes (mean ± SEM, n = 3 × 3, $, $p < 0.05$ and $$, $p < 0.01$).

(C, D, E) Distinctive ROS levels were detected by flow cytometry in *WT*, *Nrf1α*$^{-/-}$ and *Nrf2*$^{-/-}$ cell lines that had been stained by DCFH-DA (C), HPF (D), or MitoSOX (E), respectively.

(F) Different GSH levels were determined by flow cytometry in *WT*, *Nrf1α*$^{-/-}$ and *Nrf2*$^{-/-}$ cell lines that had all been stained by monochlorobimane (mBCI. Ex/Em = 394/490 nm).

(G) Relative malondialdehyde (MDA) levels were measured in WT, *Nrf1α*$^{-/-}$ and Nrf2$^{-/-}$ cells. The data are shown as fold changes (mean ± SEM, n = 3 × 3; $, $p < 0.05$ and $$, $p < 0.01$).

(H) The mRNA levels of those antioxidant genes *CAT, PRDX1, PRDX3, PRDX4, PRDX5, PRDX6, GPX1, GPX2, SOD1,* and *SOD2* were determined by RT-qPCR in WT, *Nrf1α*$^{-/-}$ and *Nrf2*$^{-/-}$ cells. The data are shown as mean ± SEM (n = 3 × 3; $, $p < 0.05$ and $$, $p < 0.01$; *, $p < 0.05$ and **, $p < 0.01$).

(I) The mRNA levels of GSH metabolism genes *GCLC, GCLM, GLS1, GSR, SLC6A9,* and *SLA7C11* were examined by RT-qPCR in *WT*, *Nrf1α*$^{-/-}$ and *Nrf2*$^{-/-}$ cells. The data are shown as mean ± SEM (n = 3 × 3; $, $p < 0.05$ and $$, $p < 0.01$; *, $p < 0.05$ and **, $p < 0.01$).

(J) The mRNA levels of *TXN1, TXN2, TXNRD1, TXNRD2* and *SRXN1* determined by RT-qPCR in *WT*, *Nrf1α*$^{-/-}$ and *Nrf2*$^{-/-}$ cells are shown as mean ± SEM (n = 3 × 3; $, $p < 0.05$ and $$, $p < 0.01$; *, $p < 0.05$ and **, $p < 0.01$).

(K) The mRNA levels of *G6PD, IDH1, IDH2, ME1, PGD* and *TIGAR* determined by RT-qPCR in *WT*, *Nrf1α*$^{-/-}$ and *Nrf2*$^{-/-}$ cells are shown as mean ± SEM (n = 3 × 3; $, $p < 0.05$ and $$, $p < 0.01$; *, $p < 0.05$ and **, $p < 0.01$).

(L) The mRNA levels of *FTH1, FTL and HO1* determined by RT-qPCR in *WT*, *Nrf1α*$^{-/-}$ and *Nrf2*$^{-/-}$ cells are shown as mean ± SEM (n = 3 × 3; $, $p < 0.05$ and $$, $p < 0.01$; *, $p < 0.05$ and **, $p < 0.01$).

(M) The mRNA levels of *SESN1, SESN2,* and *SESN3* were determined by qPCR in *WT*, *Nrf1α*$^{-/-}$ and *Nrf2*$^{-/-}$ cells. The resulting data are shown as mean ± SEM (n = 3 × 3; $, $p < 0.05$ and $$, $p < 0.01$; *, $p < 0.05$ and **, $p < 0.01$).

(N) Distinct protein levels of Nrf1, Nrf2, CAT, PRDX1, GPX1, SOD1, SOD2, TXN1, TXN2, G6PD, IDH1, IDH2, GSR, GCLM, and HO1 in *WT*, *Nrf1α*$^{-/-}$ and *Nrf2*$^{-/-}$ cells were visualized by Western blotting. The intensity of all immunoblots was also calculated as shown in Fig. S3.

excessive ROS has manifested with some pathogenic relevance to many human diseases, such as neurodegenerative, cardiovascular, inflammatory and autoimmune diseases, diabetes, aging and cancer [7].

In mammalians, Nrf1 and Nrf2 are two principal regulators of the intracellular redox homeostasis by coordinately governing transcriptional expression of distinct subsets of cognate genes through their functional heterodimers with a partner of small Maf (sMaf) or other bZIP proteins (e.g., AP-1 and ATF4), that are recruited for directly binding to those consensus sites, called antioxidant and/or electrophile response elements (AREs/EpREs), within their target promoter regions [8,9]. Both Nrf1 and Nrf2 are differentially activated in distinctive tempo-spatial responses to different extents of ROS-led oxidative stress (Figs. 1A and S1A). Under normal conditions, Nrf1 is anchored to the ER and most degraded *via* the ubiquitin-mediated proteasome pathway. When Nrf1 is required for biological responses to stimulation, this CNC-bZIP protein is allowed for dynamic dislocation from the ER lumen across membranes into extra-ER compartments, in which it is subjected to its selective proteolytic cleavage by DDI1/2 or other cytosolic proteases to become a mature transcription factor, before entering the nucleus and transactivating target genes [10,11]. By contrast, most of Nrf2 is inactive under normal conditions, because it is segregated in the cytoplasm by physic interaction with Keap1, a redox-sensitive adaptor for Cullin3, to target the second CNC-bZIP protein to the ubiquitin-mediated proteasomal degradation [12]. Once Keep is activated by increased ROS, Nrf2 is allowed for disassociation from its interactor Keap1 to enter the nucleus, where it enables to heterodimerize with sMaf and transactivate target genes.

Those antioxidant genes mediated by Nrf1 and/or Nrf2 are mainly involved in: i) glutathione production and regeneration, which are regulated by glutamate-cysteine ligase modifier (GCLM) and catalytic subunits (GCLC), glutathione reductase (GSR) [13]; ii) glutathione utilization, which is conducted by glutathione S-transferases (GSTs) and glutathione peroxidase 2 (GPXs); iii) thioredoxin production and utilization (e.g., TXNs, PRDXs); iv) NADPH production, controlled by glucose-6-phosphate dehydrogenase (G6PD), malic enzyme 1 (ME1) and isocitrate dehydrogenase 1 (IDH1) [14]; and v) the other responsible genes for antioxidant and detoxification, e.g., both encoding NAD(P)H: quinone oxidoreductase 1 (NQO1) [15] and heme oxygenase 1 (HO1) [16]. Furthermore, Nrf1 acts as a vital player in maintaining protein homeostasis (proteostasis), lipid metabolism, glucose metabolism, inflammation, cell differentiation, and embryonic development by controlling transcriptional expression of related target genes [9,17–23]. Of stinking note, Nrf2 can also exert a protective effect on normal cells against chemical carcinogens, but rather promotes cancer development and progression, particularly when it is hyper-activated for a long term [24,25]. By contrast, Nrf1α (and long isoform TCF11) is identified as a potent tumor-repressor to inhibit cancer malgrowth in xenograft model mice [26]. This is supported by liver-specific knockout of Nrf1 in mice with obvious pathological phenotypes, resembling human non-alcoholic steatohepatitis (NASH) and hepatoma [27,28]. Our previous evidence also revealed that knockout of Nrf1 from human hepatoma cells results in the exacerbation of tumor growth and migration, but such malignant growth appears to be strikingly prevented upon overexpression of Nrf1α or TCF11 [26,29].

In this study, we found that knockout of Nrf1α (a major full-length isoform of prototypic Nrf1) caused a substantial increase of the intracellular ROS determined in *Nrf1α*$^{-/-}$ cells, when compared with wild-type (*WT*) and *Nrf2*$^{-/-}$cells. Such increased ROS levels were accompanied by up-regulation of most genes responsible for antioxidant and detoxification; this is attributable to aberrant accumulation of Nrf2 upon loss of Nrf1α. Interestingly, abnormal changes in the mitochondrial morphology of *Nrf1α*$^{-/-}$ rather than *Nrf2*$^{-/-}$ cells were observed, as accompanied by impaired ETC complexes. Further examinations also unraveled that *Nrf1α*$^{-/-}$-derived mitochondrial dysfunction was owing to deregulation of two nuclear respiratory factors αPal^{NRF1} (nuclear respiratory factor 1) and GABPα^{NRF2} (nuclear respiratory factor 2), along with the co-factor PGC1α, resulting in strikingly increased ROS levels in *Nrf1α*-deficient cells. Besides, glycolysis of *Nrf1α*$^{-/-}$ cells was greatly augmented by hyperactive Nrf2, leading to an aggravated pressure of mitochondrial stress. The mitochondrial UCP2 was markedly suppressed by Nrf2 through AREs-driven miR-195 and miR-497. These collectively contribute to a drastic increase of ROS in *Nrf1α*$^{-/-}$ cells; this is concomitant with the activation of multiple signaling pathways *via* MAPK, PI3K-AKT, HIF1α, and NF-κB to the EMT process involved in cancer development and progression. Overall, Nrf1 acts as a vital player in determining and maintaining robust redox homeostasis by governing mitochondrial homeostasis integrated from multi-hierarchical signaling pathways towards cognate gene regulatory networks. Therefore, this work provides a novel understanding of the distinct roles of Nrf1 and Nrf2 in cancer development and prevention.

2. Materials and methods

2.1. Cell lines, culture and transfection

Nrf1α$^{-/-}$ cells were established by TALENs-led genome editing with HepG2 cells [26], whereas *Nrf2*$^{-/-}$ cells were constructed by CRISPR/Cas9-editing system with HepG2 cells [29]. These cell lines expressing Nrf1α and Nrf2, as well as an empty control, were established by using the Flp-In™ TREx™-293 system with HepG2 cells (Invitrogen) [30]. These cell lines were maintained in DMEM supplemented with 5 mM glutamine, 10% (v/v) fetal bovine serum (FBS), and 100 units/mL of either penicillin or streptomycin, in the 37 °C incubators with 5% CO_2. **In addition, some** cell lines were transfected for 8 h with the indicated constructs mixed with the Lipofectamine®3000 agent in the Opti-MEM (gibca, Waltham, MA, USA). The cells were then allowed for recovery from transfection in a fresh complete medium for 24 h before the other experiments were conducted.

2.2. Plasmid construction

The expression constructs for human Nrf1 and Nrf2 were created by inserting their full-length cDNA sequences into the KpnI/XbaI site of pcDNA3.1/V5His B. The six reporter gene plasmids for PGC1α-luc, αPal^{NRF1}-luc, GABPα-luc, UCP2-luc, miR-195-luc and miR-497-luc were created by inserting their promoter sequences into the PGL3-basic vector, distinct lengths of each gene promoter are indicated in Figs. 3E and 5H. In addition, the *ARE*-luc plasmids were created by inserting the consensus *ARE*-adjoining sequences (Figs. 3G and 5J) from indicated gene promoters into the PGL3-promoter vector. The 3'-UTR of UCP2 was cloned into the psiCHECK-2 plasmid.

2.3. Real-time qPCR analysis of mRNA expression

Their total RNAs were extracted by using an RNA extraction kit (TIANGEN, Beijing, China), then approximately 2.0 μg of total RNAs were added in a reverse-transcriptase reaction to generate the first strand of cDNA (by using the Revert Aid First Strand Synthesis Kit, Thermo, Waltham, MA, USA). The synthesized cDNA served as the template for qPCR, in the GoTaq®qPCR Master Mix (Promega, Madison, WI, USA). Subsequently, relative mRNA expression levels were measured by qRT-PCR with indicated pairs of primers. Of note, the mRNA expression level of β-actin served as an optimal internal standard control, relative to other mRNA expression levels presented as fold changes. All the forward and reverse primers of those indicated genes were shown in Table S1.

2.4. Western blotting (WB)

Experimental cells were harvested in a denatured lysis buffer (0.5% SDS, 0.04 mol/L DTT, pH 7.5, containing 1 tablet of cOmplete protease inhibitor EASYpacks in 10 ml of this buffer). The total lysates were

further denatured by boiling at 100 °C for 10 min, sonicated sufficiently, and diluted with 3 × loading buffer (187.5 mmol/L Tris-HCl, pH 6.8, 6% SDS, 30% Glycerol, 150 mmol/L DTT, 0.3% Bromphenol Blue), before being re-boiled at 100 °C for 5 min. Thereafter, equal amounts of protein extracts were subjected to separation SDS-PAGE before being transferred to polyvinylidene fluoride (PVDF) membranes (Millipore, Billerica, MA, USA), and subsequent visualization by Western blotting with distinct antibodies as indicated. β-actin served as an internal control to verify equal loading of proteins in each of the electrophoretic wells.

2.5. Intracellular ROS and GSH detection

Experimental cells were incubated in a serum-free medium containing 20,70-Dichlorodihydrofluorescein diacetate (DCFH-DA, S0033, Beyotime, Shanghai, China), 3'-(p-hydroxyphenyl) fluorescein (HPA, H36004, ThermoFisher), MitoSOX Red (40778ES50, Yeasen Biotechnology, Shanghai, China) or Monochlorobimane (mBCL, HY-101899, MedChemExpress) at 37 °C for 20 min. After the cells were washed three times with a fresh serum-free medium, the relevant fluorescence intensity is measured by a flow cytometer or fluorescent inverted microscope in specific excitation (Ex) and emission (Em) lights. Among them, Ex/Em of DCFH-DA is 488/525 nm, Ex/Em of HPF is 490/515 nm, and Ex/Em of MitoSOX is 510/580 nm, Ex/Em of Monochlorobimane is 380/470 nm.

2.6. MDA, pyruvate, triglyceride and ATP content detection

Both MDA and ATP levels were determined, respectively, according to the instruction of an enhanced ATP assay kit and another kit of lipid oxidation (MDA) detection (both kits from Beyotime, Shanghai, China). The pyruvate and triglyceride contents were measured according to their respective assay kits (from Njjcbio, Nanjing, china).

2.7. CHIP-sequencing analysis

The CHIP-sequencing data was analyzed by Encode database (https://www.encodeproject.org). The project numbers in Encode were ENCSR543SBE (Nfe2l1 in HepG2 cells) and ENCSR488EES (Nfe2l2 in HepG2 cells).

2.8. Luciferase reporter assay

Equal numbers (1.0×10^5) of COS1 cells were allowed for growth in each well of 12-well plates. After reaching 70–80% confluence, the cells were co-transfected for 8 h with an indicated luciferase plasmid alone or together with one of the expression constructs with the Lipofectamine®3000 agent in the Opti-MEM (gibca, Waltham, MA, USA) the Renilla-expressing pRL-TK plasmid served as an internal control for transfection efficiency. After being cultured in a fresh complete medium for 24 h, the cells were lysed and then the luciferase activity was measured by the dual-reporter assay (Promega, Madison, WI, USA).

2.9. Transmission electron microscopy

Experimental cells were pelleted by centrifuging (1000 rpm) before being fixed with 2.5% glutaraldehyde in 0.1 M sodium cacodylate buffer pH 7.4 for 30 min at 37 °C. The fixed cells stored in 4 °C in 0.1 M sodium cacodylate buffer were performed with a mixture of 1% OsO4, 1.5% K4Fe(CN)6 in 0.1 M sodium cacodylate pH 7.4 for 1 h at 4 °C and then overnight incubated in 0.25% uranyl acetate at 4 °C. After three water washes, samples were dehydrated in series of 15 min steps in 25%, 50%, 75%, 95% and 100% (v/v) ethanol and embedded in an epoxy resin (Sigma-Aldrich). The ultrathin sections (of 60–70 nm in thickness) of cells were prepared with a Leica EM UC7 ultramicrotome and counterstained with 1% uranyl acetate for 15 min and 1% lead citrate for 6 min. Thin sections were imaged using a HITACHI HT 7800 120kv transmission electron microscope operating at 80 kV.

2.10. Flow cytometry analysis of apoptosis

Experimental cells (3×10^5) were allowed for growth in each well of 6-well plates. After transfection or drug treatment, the cells were pelleted by centrifuging at 1000×*g* for 5 min and washed with PBS for three times, before being incubated for 15 min with 5 μL of Annexin V-FITC and 10 μL of propidium iodide (PI) in 195 μL of the binding buffer. The results were analyzed by the FlowJo 7.6.1 software (FlowJo, Ashland, OR, USA) before being presented.

2.11. The transwell-based migration and invasion assays

The Transwell-based migration and invasion assays were conducted in the modified Boyden chambers (Transwell; Corning Inc. Lowell, MA, USA). Equal numbers of cells were allowed for growth in each well of 12-well plates. After reaching 70–80% confluence, they were starved for 12 h in a serum-free medium. The experimental cells (1×10^4) were suspended in a 0.5 ml medium containing 5% FBS and seeded in the upper chamber of a Transwell. The cell-seeded Transwells were placed in each well of 24-well plates containing 1 ml of complete medium (i.e., the lower chamber), and then cultured for 24 h in the incubator at 37 °C with 5% CO2. Of note, the bottom of the upper Transwell was pre-coated by matrigel basement matrix (BD, Biosciences, USA), before the cells were placed in the invasion assay. The remaining cells in the upper chamber were removed, and the cells attached to the lower surface of the Transwell membranes were fixed with 4% paraformaldehyde (AR10669, BOSTER) and stained with 1% crystal violet reagent (Sigma) before being counted.

2.12. Statistical analysis

Statistical significance of changes in the reporter gene activity or other gene expression was determined using either the Student's *t*-test or Multiple Analysis of Variations (MANOVA). The resulting data are shown as a fold change (mean ± S.D), each of which represents at least 3 independent experiments that were each performed triplicate.

3. Results

3.1. A dramatic increase of ROS results from loss of Nrf1α, but is not eliminated by hyperactive Nrf2 in *Nrf1α*$^{-/-}$ cells

Albeit it was previously reported that the intracellular ROS levels were increased in mouse *Nrf1*-and *Nrf2*-deficient cells [31], the underlying mechanism remains elusive, to date. Contrarily, Nrf2 was also shown to amplify oxidative stress by induction of Kruppel-like factor 9 (KLF9) in response to elevated ROS over the presetting threshold [32]. To gain an insight into the distinct roles of Nrf1 and Nrf2 in determining and maintaining redox homeostasis, we reexamined human *Nrf1α*$^{-/-}$ and *Nrf2*$^{-/-}$cell lines; both were established by the genomic editing of HepG2 cells [26,29]. Here, we found that knockout of either *Nrf1α*$^{-/-}$ or *Nrf2*$^{-/-}$ caused an obvious increase in their intracellular ROS levels (detected by DCFH-DA, as the most commonly used probe with a relatively large range from detecting H_2O_2, $O_2^{\cdot-}$,·OH to $ONOO^-$), but the increased ROS in *Nrf1α*$^{-/-}$ cells were significantly higher than those in *Nrf2*$^{-/-}$ cells (Figs. 1B and 1C). To confirm this result, two additional fluorescent probes HPF (hydroxyphenyl fluorescein, sensing particularly to intracellular $O_2^{\cdot-}$ and $ONOO^-$ changes) and MitoSOX (specifically sensing to mitochondrial $O_2^{\cdot-}$ changes) were also employed (Fig. S1B). The resulting data revealed that distinct extents of the increased ROS in between *Nrf1α*$^{-/-}$ and *Nrf2*$^{-/-}$ cell lines were amplified by HPF (Fig. 1D). However, it is, to our surprise, found that almost no changes in the mitochondrial $O_2^{\cdot-}$-sensing fluorescence were detected by MitoSOX in *Nrf2*$^{-/-}$cells, but *Nrf1α*$^{-/-}$ cells were manifested with a significant

magnitude of its mitochondrial ROS (Fig. 1E) when compared to *WT* controls. A concomitant decrease in the reduced glutathione (GSH, as a free radical scavenger and potent detoxifying agent) was also determined in *WT*, *Nrf1α*$^{-/-}$ and *Nrf2*$^{-/-}$ cell lines (Figs. 1F, S1C); this is negatively correlated with the intracellular ROS levels, as described [33]. As such, further examination of malondialdehyde (MDA, a marker of polyunsaturated fatty acids peroxidation in the cell) unraveled a substantially increased production in *Nrf1α*$^{-/-}$ cells, to 8 times higher than that obtained from *WT* cells, whereas *Nrf2*$^{-/-}$ cells only displayed ~2-fold changes (Fig. 1G). Collectively, these demonstrate that loss of *Nrf1α* has led to severe endogenous oxidative distress which may be caused primarily by increased ROS from mitochondria, and, by contrast, loss of *Nrf2* only causes modest oxidative stress in the presence of *Nrf1*.

To explore the reasons underlying such distinct increases of ROS caused by deficiency of *Nrf1α* from *Nrf2*, it was surprisingly unveiled by transcriptome sequencing that most of those differential expression genes responsible for antioxidant and detoxification were significantly up-regulated in *Nrf1α*$^{-/-}$cells, but also markedly down-regulated in *Nrf2*$^{-/-}$ cells (Fig. S2), when compared to *WT* cells. Further quantitative PCR of critical genes for ROS elimination revealed that *Nrf1α*$^{-/-}$cells gave rise to obvious increases in basal expression of *SOD2* (superoxide dismutase 2, converting the mitochondrial $O_2^{\cdot-}$ into H_2O_2), *PRDX1, PRDX4, PRDX5* (peroxiredoxins, all three scavenging H_2O_2 by consuming reduced thioredoxin) and *GPX1* (glutathione peroxidase 1), but extra-mitochondrial *SOD1* expression was decreased (Fig. 1H). Conversely, *Nrf2*$^{-/-}$ cells manifested significantly decreased expression of *SOD2, PRDX5* and *GPX1*, but *PRDX4* was highly expressed, while *SOD1* was modestly increased. Also, it was, much to our surprise, found that basal expression of those examined genes *GCLC, GCLM, GLS* (*glutaminase*), *GSR, SLC6A9* and particularly *SLC7A11* (all involved in GSH biosynthesis and regeneration) was significantly up-regulated in *Nrf1α*$^{-/-}$cells, but down-regulated in *Nrf2*$^{-/-}$ cells, when compared with *WT* controls (Fig. 1I). Additional two reducing powers *TXN* (thioredoxin) and *TXN2* (thioredoxin-2) were up-expressed in *Nrf1α*$^{-/-}$cells, but down-expressed in *Nrf2*$^{-/-}$ cells, whereas basal expression of *TXNRD1* (thioredoxin reductase-1) and *TXNRD2* (thioredoxin reductase-2) was almost not changed in both cell lines (Fig. 1J). Moreover, basal expression of *SRXN1* (sulfiredoxin 1) was reduced only in *Nrf2*$^{-/-}$cells, but largely unaltered in *Nrf1α*$^{-/-}$cells (Fig. 1J). Collectively, these findings demonstrate that loss of *Nrf2* results in obvious defects in *de novo* biosynthesis of GSH and TXN and their recycling, but rather unusual increases of them have strikingly emerged upon loss of *Nrf1α*.

Further examination revealed that basal expression of *G6PD* (glucose-6-phosphate dehydrogenase, a key enzyme in the pentose phosphate pathway to yield NADPH) and *PGD* (6-phosphogluconate dehydrogenase, as the second dehydrogenase in the pentose phosphate shunt) was slightly increased or unaltered in *Nrf1α*$^{-/-}$cells respectively, but decreased in *Nrf2*$^{-/-}$ cells (Fig. 1K). Conversely, significant increases in basal *TIGAR* (TP53 induced glycolysis regulatory phosphatase, blocking glycolysis and directing the pathway into the pentose phosphate shunt to protect cells from DNA-damaging ROS) expression were observed in both *Nrf1α*$^{-/-}$ and *Nrf2*$^{-/-}$ cell lines (Fig. 1K). Besides, basal expression of *ME1* (malic enzyme, as another NADPH supplier) was also substantially up-regulated in *Nrf1α*$^{-/-}$cells to ~4-fold changes higher than its *WT* control, but almost unchanged in *Nrf2*$^{-/-}$ cells. By contrast, *IDH1* (isocitrate dehydrogenase, a key enzyme catalyzing the oxidative decarboxylation of isocitrate to alpha-ketoglutarate to generate CO_2 and NADPH in the citric acid cycle), rather than *IDH2*, was significantly lowered in *Nrf1α*$^{-/-}$cells, but highly expressed in *Nrf2*$^{-/-}$ cells (Fig. 1K). Altogether, these indicate knockout of *Nrf1α* leads to a redox metabolism reprogramming, that is distinctive from the knockout of *Nrf2*.

Next, by quantitative investigation of another antioxidant capability to prevent free heme from forming free radicals during oxidative stress [16], it was unraveled that basal expression levels of *HO1* and *FTH1* (ferritin heavy chain) were up-regulated in *Nrf1α*$^{-/-}$cells, but down-regulated in *Nrf2*$^{-/-}$ cells (Fig 1L), while no changes in the expression of *FTL* (ferritin light chain) were observed in both cell lines when compared to *WT* controls. In addition, another potent antioxidant family of highly conserved sestrin (SESN, involved in the reduction of PRDXs, so to negatively regulate mTORC signaling pathways was also investigated herein) [34]. Among them, *SESN1* was up-expressed in both *Nrf1α*$^{-/-}$and *Nrf2*$^{-/-}$ cell lines, whereas *SESN2* was only up-expressed in *Nrf1α*$^{-/-}$ cells, but rather down-expressed in *Nrf2*$^{-/-}$ cells (Fig 1M). By sharp contrast, basal expression of *SESN3* was significantly down-regulated in *Nrf1α*$^{-/-}$ cells and also almost abolished in *Nrf2*$^{-/-}$ cells when compared with *WT* controls. These imply distinct roles for Nrf1α and Nrf2 in governing antioxidant potentials and also redox signaling to mTORC-regulated networks to meet the needs of cell survival.

Further insights into the protein expression of critical genes by Western blotting revealed that, albeit the processed Nrf1-C/D isoform is only slightly decreased in *Nrf2*$^{-/-}$ cells, basal Nrf2 protein was aberrantly, substantially accumulated in *Nrf1α*$^{-/-}$ cells (Fig 1N and S3), as consistent with our previous results [29,35]. Such hyperactive Nrf2 should be interpreted as a compensation for loss of Nrf1, and consequently attributable to the constant up-regulation of most antioxidant and detoxifying genes in *Nrf1α*$^{-/-}$ cells. As anticipated, most of the examined proteins including CAT (catalase), PRDX1, GPX1, SOD2, TXN1, TXN2, G6PD, GSR, GCLM and HO1 were highly expressed as accompanied by hyperactive Nrf2 accumulation in *Nrf1α*$^{-/-}$ cells (Figs 1N and S3). However, basal abundances of SOD1 and IDH1, rather than IDH2, were down-regulated in *Nrf1α*$^{-/-}$ cells, but almost unaffected in *Nrf2*$^{-/-}$ cells, implying they may serve as Nrf1-specific targets.

3.2. Loss of Nrf1α results in mitochondrial dysfunction and oxidative damage in Nrf1α$^{-/-}$ cells

Intriguingly, the above-described data indicate that even though hyperactive Nrf2 accumulated with up-regulation of antioxidant and detoxification genes, *Nrf1α*$^{-/-}$ cells are still manifested with severe endogenous oxidative stress, caused primarily by ROS yielded from its mitochondria, but rather not similar distress has been suffered from *Nrf2*$^{-/-}$ cells. To address this, we herein examine distinct subunits of mitochondrial ETC complexes I to IV in *Nrf1α*$^{-/-}$ cells, by comparison with *Nrf2*$^{-/-}$ cells and *WT* controls. As anticipated, most subunits of the mitochondrial respiratory chain were, to different extents, down-regulated in *Nrf1α*$^{-/-}$ cells (Fig. 2A). By contrast, their mRNA expression in *Nrf2*$^{-/-}$ cells appeared to be unaffected or slightly enhanced, with an exception of *SDHA* (succinate dehydrogenase complex flavoprotein subunit A). Of note, *ND1*, *MTCYB*, *MTCO1* and *MTCO2* are encoded by the mitochondrial genome *per se*, all other examined subunits are encoded by the nuclearly-located genes. Western blotting also revealed that protein abundances of NDUFC2, SDHA, SDHB, NQCRFS1, MTCO1, and MTCO2 were decreased in *Nrf1α*$^{-/-}$, but not *Nrf2*$^{-/-}$, cell lines (Fig. 2B). These demonstrate that loss of *Nrf1α*, rather than *Nrf2*, leads to a certain dysfunction of the mitochondrial respiratory chain.

Next, treatment of *WT* cells with rotenone (a specific inhibitor of mitochondrial ETC complex I [36]) unraveled that the intracellular oxidative stress was aggravated by incrementing the mitochondrial ROS production in a time-dependent manner (Fig. 2C, *left panel*), albeit Nrf2 protein expression was enhanced by this chemical (Fig. S4A). Rather, similar rotenone treatment of *Nrf1α*$^{-/-}$ cells rendered its severe endogenous oxidative stress to be significantly mitigated to a certain extent (Fig. 2C, *middle panel*), but roughly no obvious changes were determined after treatment of *Nrf2*$^{-/-}$ cells (Fig. 2C, *right panel*). Also, no significant differences in rotenone-induced apoptosis were observed in these three cell lines (Figs S4B and S4C). These indicate that *Nrf1α*$^{-/-}$-derived dysfunction of its mitochondrial respiratory chain to give rise to considerable higher ROS levels is not further worsened but conversely relieved by rotenone, while not a similar event appears to take place in

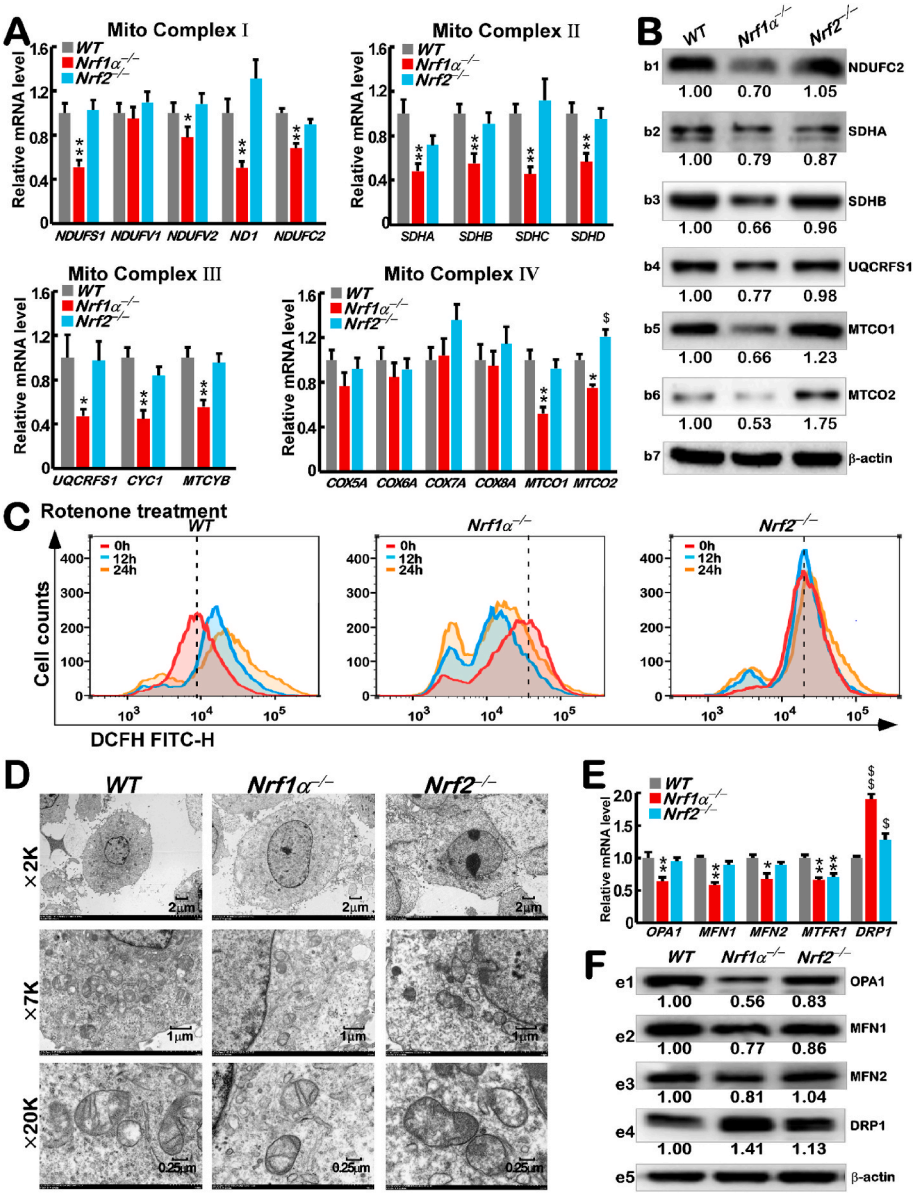

Fig. 2. Changes in mitochondrial genes and morphology of *Nrf1α*$^{-/-}$ distinctive from *Nrf2*$^{-/-}$ cells

(A) The mRNA levels of *NDUFS1, NDUFV1, NDUFV2, ND1, NDUFC2, SDHA, SDHB, SDHC, SDHD, UQCRFS1, CYC1, MTCYB, COX5A, COX6A, COX7A, COX8A, MTCO1,* and *MTCO2* were determined by RT-qPCR in *WT*, *Nrf1α*$^{-/-}$ and *Nrf2*$^{-/-}$ cells. The resulting data are shown as mean ± SEM (n = 3 × 3; *, $p < 0.05$ and **, $p < 0.01$).

(B) The protein expression levels of NDUFC2, SDHA, SDHB, NQCRFS1, MTCO1, and MTCO2 in *WT*, *Nrf1α*$^{-/-}$ and *Nrf2*$^{-/-}$ cells were visualized by Western blotting. The intensity of all the immunoblots was calculated and shown on the bottom.

(C) Distinct ROS levels and detected by flow cytometry in *WT*, *Nrf1α*$^{-/-}$ and *Nrf2*$^{-/-}$ cells that had been treated with Rotenone for 0 h, 12 h, or 24 h and then stained by DCFH for 30 min.

(D) The electronic micrographs representative of *WT*, *Nrf1α*$^{-/-}$ and *Nrf2*$^{-/-}$ cells. The scale bar = 2 μm in × 2 K pictures, or = 1 μm in × 7 K pictures, or = 0.25 μm in × 20 K pictures.

(E) Differential mRNA expression levels of *Drp1, OPA1, MFN1, MFN2* and *MTFR1* determined by RT-qPCR in *WT*, *Nrf1α*$^{-/-}$ and *Nrf2*$^{-/-}$ cells are shown as mean ± SEM (n = 3 × 3; $, $p < 0.05$ and $$, $p < 0.01$; *, $p < 0.05$ and **, $p < 0.01$).

(F) The protein levels of OPA1, MFN1, MFN2, and Drp1 in *WT*, *Nrf1α*$^{-/-}$ and *Nrf2*$^{-/-}$ cells were visualized by Western blotting. The intensity of all the immunoblots was calculated and shown on the bottom.

Nrf2$^{-/-}$ cells. In addition, rotenone could only reduce a small amount of ATP production while glycolysis inhibitors 2-DG could reduce most ATP production in *Nrf1α*$^{-/-}$ cells (Figs. S5A and 5B); this indicates that ATP is mainly supplied by glycolysis after Nrf1 knockout.

Electron micrographic imaging showed that morphological changes of *Nrf1α*$^{-/-}$ cells were distinctive from *Nrf2*$^{-/-}$ cells (Figs. 2D and S5C). The mitochondria of *Nrf1α*$^{-/-}$ cells seem to be shrunk, with significant decreases in their mitochondrial number and their cristae in each mitochondrion (*middle panels*), whereas the mitochondria of *Nrf2*$^{-/-}$ cells appeared to be modestly reinforced (*right panels*) when compared with *WT* cells (*left panels*). Further examination of critical players in the mitochondrial fission and fusion (for maintaining a steady state of mitochondrial function under cellular metabolic or environmental stress [37])by RT-PCR and Western blotting revealed that *MFN1* (mitofusin 1) and *OPA1* (optic atrophy 1, serving mitochondrial dynamin-like GTPase) were down-regulated in *Nrf1α*$^{-/-}$ cells (Figs. 2E and 2F). By contrast, *DRP1* (dynamin-related protein 1, a key regulator of mitochondrial division) was substantially up-regulated in *Nrf1α*$^{-/-}$ cells, even though *MTFR1* (mitochondrial fission regulator 1) was decreased. However, slight changes in these players were examined in *Nrf2*$^{-/-}$ cells. Altogether, loss of *Nrf1α* results in dysfunctional mitochondria, thereby producing considerably higher levels of ROS along with oxidative damages.

3.3. *Nrf1 directly regulates two nuclear respiratory factors αPal*^{NRF1} *and GABPα*^{NRF2}*, and co-factor PGC1α*

To gain an insight into the underlying mechanism for mitochondrial dysfunction caused by loss of *Nrf1α*$^{-/-}$, we here examined the constitutive expression of two nuclear respiratory factors αPal^{NRF1} and GABPα^{NRF2} [38,39], cofactor PGC1α, and critical target genes (responsible for mitochondrial DNA replication and transcription, ETC/OXPHOS gene expression, and mitochondrial biogenesis [40]). The results showed that basal mRNA expression levels of *αPal*^{NRF1}, *GABPα*^{NRF2} and co-targeting mitochondrial transcription factors *TFAM* (transcription factor A, mitochondrial), *TFB1M* (transcription factor B1, mitochondrial) and *TFB2M* (transcription factor B2, mitochondrial), together with *PGC1α*, but not *PGC1β*, were down-regulated, though to different extents, in *Nrf1α*$^{-/-}$ cells (Fig. 3A). However, such key factors *αPal*^{NRF1} and *GABPα*^{NRF2} were not significantly affected in *Nrf2*$^{-/-}$ cells, which only

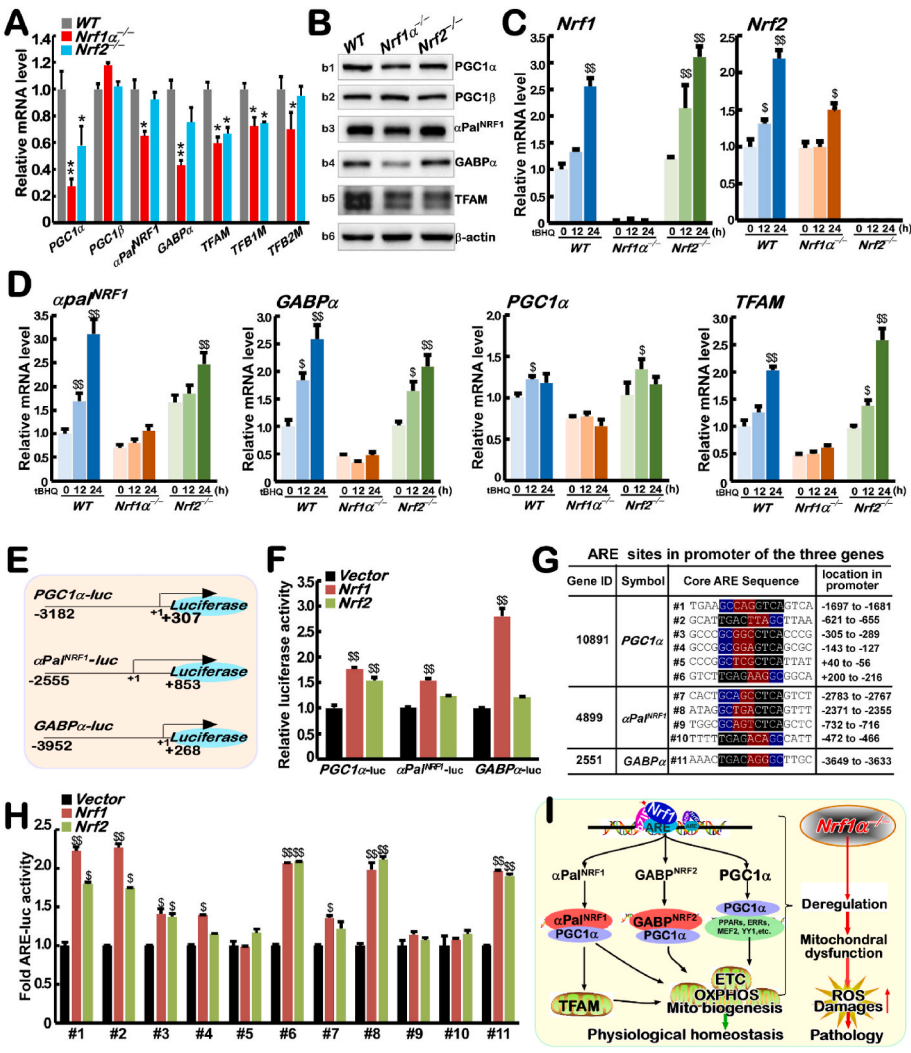

Fig. 3. Distinct effects of Nrf1 and Nrf2 on nuclearly-controlled mitochondrial factors PGC1α, PGC1β, αPal^{NRF1}, GABPα

(A) The mRNA expression levels of *PGC1α, PGC1β, αPal^{NRF1}, GABPα, TFAM, TFB1M,* and *TFB2M* were determined by RT-qPCR in *WT*, *Nrf1α*$^{-/-}$ and *Nrf2*$^{-/-}$ cells. The data are shown as fold changes (mean ± SEM, n = 3 × 3; *, p < 0.05 and **, p < 0.01).

(B) The protein levels of PGC1α, PGC1β, αPal^{NRF1}, GABPα, and TFAM in *WT*, *Nrf1α*$^{-/-}$ and *Nrf2*$^{-/-}$ cells were visualized by Western blotting. The intensity of all the immunoblots was calculated and shown in Fig. S6A.

(C) The mRNA levels of *Nrf1* and *Nrf2* were determined by RT-qPCR in *WT*, *Nrf1α*$^{-/-}$ and *Nrf2*$^{-/-}$ cells, which had been treated with tBHQ for 0 h, 12 h, or 24 h. The data are shown as mean ± SEM (n = 3 × 3) with significant increases ($, p < 0.05 and $$, p < 0.01) as compared to the cells without this chemical treatment.

(D) The mRNA levels of *αpal^{NRF1}, GABPα, PGC1α,* and *TFAM* were determined by RT-qPCR in *WT*, *Nrf1α*$^{-/-}$ and *Nrf2*$^{-/-}$ cells, which had been treated with tBHQ for 0 h, 12 h, or 24 h. The resulting data are shown above.

(E) Schematic representation of the *PGC1α-luc, αPal^{NRF1}-luc,* and *GABPα-luc*, which were constructed into the PGL3-Promoter plasmid. Their promoter regions were also indicated.

(F) Relative luciferase activity of *PGC1α-luc, αPal^{NRF1}-luc,* and *GABPα-luc* were determined in COS-1 cells that had been co-expressed with each reporter gene and pRL-TK (as an internal reference), plus an expression construct for Nrf1 or Nrf2, or empty pcDNA3 vector. The data are shown as mean ± SEM (n = 3 × 3; $, p < 0.05 and $$, p < 0.01).

(G) The consensus ARE sites within the promoter of *PGC1α, αPal^{NRF1},* and *GABPα* were listed herein.

(H) Fold *ARE-luc* activity mediated by Nrf1 or Nrf2 was determined. The indicated *ARE*-adjoining sequences were cloned into the PGL3-promoter vector, and were co-expressed with pRL-TK, plus expression constructs for Nrf1 or Nrf2, or empty pcDNA3 plasmid, then operated as above.

(I) A proposed model that Nrf1 and Nrf2 regulate mitochondrial function by *αpal^{NRF1}, GABPα,* and *PGC1α.*

gave rise to marginally decreased expression of *PGC1α*, *TFAM*, *TFB1M*, but not *TFB2M*. Further examinations also revealed that basal abundances of αPal^{NRF1}, GABPα^{NRF2}, PGC1α and TFAM proteins were down-regulated in *Nrf1α*$^{-/-}$ cells, while in *Nrf2*$^{-/-}$ cells only TFAM was down-expressed (Figs. 3B and S6A). Collectively, these indicate that *Nrf1α*$^{-/-}$-caused mitochondrial dysfunction is attributable to deregulation of nuclear respiratory controls towards the mitochondrial gene transcriptional networks. This is also further supported by the restoration of ectopic Nrf1 factor into *Nrf1α*$^{-/-}$ cells (Fig. S6B), showing greater or lesser extents of recovery of those four key factors (αPal^{NRF1}, GABPα^{NRF2}, PGC1α and TFAM), together with other mitochondrial proteins NDUFC2, NQCRFS1, MTCO1, MTCO2, and SDHB, but not SDHA. Additional supportive evidence was obtained from the tetracycline-inducible Nrf1-expressing cell lines (Figs. S6C and S6D), in which almost all those examined mRNAs and proteins were up-regulated. By contrast, Nrf2 induction by tetracycline led to significantly increased expression of PGC1α, GABPα^{NRF2} and TFAM, besides HO1 and GCLM. This implies at least a partial involvement of Nrf2 in regulating the mitochondrial function, particularly when it is required for certain inducible cues.

To further investigate distinct roles for Nrf1 and Nrf2 in the nuclear-to-mitochondrial regulation, the experimental *Nrf1α*$^{-/-}$, *Nrf2*$^{-/-}$, and *WT* cell lines were treated with *tert*-butylhydroquinone (*t*BHQ, as a pro-oxidative stressor [41]). The results revealed that *Nrf1, Nrf2, PGC1α, αPal^{NRF1}, GABPα^{NRF2},* and *TFAM* (Figs. 3C & 3D and S7A & S7B) along with *HO1* and *GCLM* (Fig. S7C) were significantly induced by *t*BHQ stimulation in *WT* cells. Such induction of *PGC1α, αPal^{NRF1}, GABPα^{NRF2}* and *TFAM* (controlling the mitochondrial function) was almost completely abolished in *Nrf1α*$^{-/-}$ cells (Fig. 3C), even albeit hyperactive Nrf2 and its targeting HO1 and GCLM were further enhanced by *t*BHQ (Figs. S7A–C). Conversely, although induction of HO1 and GCLM by *t*BHQ was abolished in *Nrf2*$^{-/-}$ cells, different inducible extents of *αPal^{NRF1}, GABPα^{NRF2}, TFAM* and *PGC1α* were still stimulated by this chemical, and also accompanied by induction of Nrf1 in *Nrf2*-deficient cells. Taken altogether, these demonstrate that Nrf1 rather than Nrf2 is essential for maintaining mitochondrial functional homeostasis by governing the nuclear respiratory factors.

To clarify whether Nrf1 or Nrf2 directly regulates such key genes *αPal^{NRF1}, GABPα^{NRF2}* and *PGC1α*, their promoter regions were constructed into relevant luciferase reporters (as shown in Fig. 3E). The results revealed that these reporter genes *αPal^{NRF1}-Luc, GABPα^{NRF2}-Luc* and *PGC1α-Luc* were transcriptionally activated by ectopic expression of

Nrf1 (Fig. 3F). Of note, transactivation activity of $GABP\alpha^{NRF2}$-*Luc* mediated by Nrf1 was substantially increased to ~2.5 times over its control values. By contrast, Nrf2 only gave rise to marginal transactivation of these reporter genes at considerably lower levels. Further sequence analysis unraveled that several *ARE* consensus sites are present in the promoter regions of αPal^{NRF1}, $GABP\alpha^{NRF2}$ and *PGC1α*, respectively (Fig. 3G). Some of such *ARE*-driven luciferase reporter genes (with ARE site of HO1 acting as a positive control) were also *trans*-activated by Nrf1 and/or Nrf2 (Figs. 3H and S7D). In search of the Encode database, the ChIP-sequencing data for binding Nrf1 and Nrf2 in HepG2 cells failed to show significant signals in the promoter regions of αPal^{NRF1}, $GABP\alpha^{NRF2}$, and *PGC1α*, because signals are considerably weak (Fig. S8), while further validation is needed. Overall, these results suggest that Nrf1 (alongside with Nrf2) in a combination with putative DNA-binding partners or other cofactors regulates αPal^{NRF1}, $GABP\alpha^{NRF2}$ and *PGC1α* for determining mitochondrial homeostasis (Fig. 3I). But, conversely loss of $Nrf1\alpha^{-/-}$ leads to a fatal defect in this critical gene expression, resulting in mitochondrial dysfunction and oxidative damages.

3.4. Glycolysis of $Nrf1\alpha^{-/-}$ cells is enhanced to aggravate its mitochondrial pressure with increased ROS production

Since as by-products of mitochondrial oxidative metabolism, ROS are allowed to connect with controls of metabolic process, such that the yield of ROS in this organelle depends on distinct types of fuel loading (carbohydrate, lipid, protein), besides mitochondrial functional homeostasis *per se* [42]. Here, transcriptomic sequencing analysis revealed significant differential expression of those genes responsible for energy metabolism, as well as carbohydrate and lipid metabolisms of $Nrf1\alpha^{-/-}$ cells (Fig. S9), but these metabolic gene changes were strikingly diminished, abolished, or even reversed in $Nrf2^{-/-}$ cells. Thereafter, $Nrf1\alpha^{-/-}$, $Nrf2^{-/-}$ and *WT* cell lines had been allowed for growth in a complete medium containing 25 mM *versus* 5 mM glucose for 24 h, before the putative effect of glucose, as a fuel load, on the amount of intracellular ROS production was determined. As shown in Fig. 4A, the ROS levels detected by flow cytometry of *WT* cells fed with 25 mM glucose were augmented when compared with those arising from 5 mM glucose conditions. Such a supply of 25 mM glucose deteriorated endogenous oxidative stress in $Nrf1\alpha^{-/-}$ cells (*middle panel*), whereas $Nrf2^{-/-}$ cells appeared to be unaffected (*right panel*). Conversely,

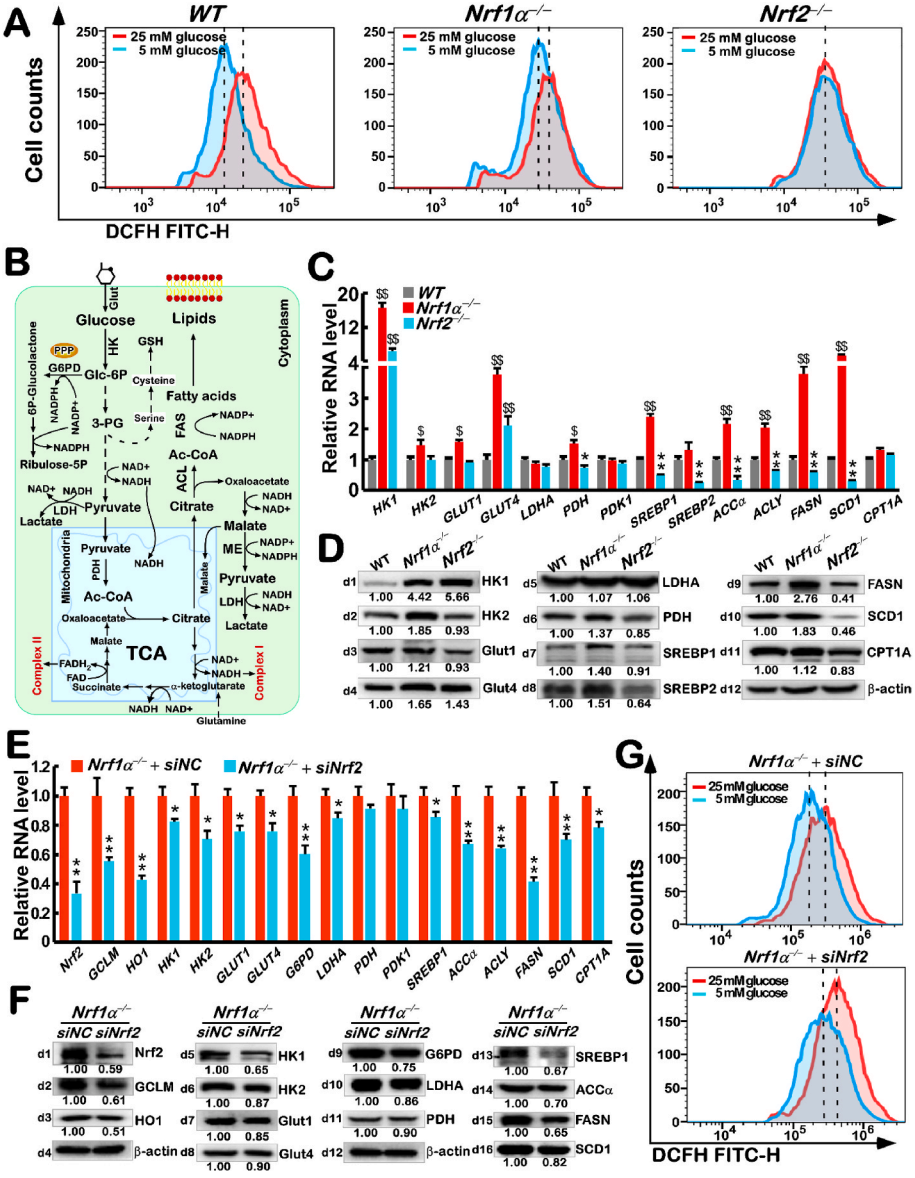

Fig. 4. Changes in ROS levels arising from differential expression of redox metabolic genes in $Nrf1\alpha^{-/-}$ and $Nrf2^{-/-}$ cells lines.

(A) Changes in ROS levels were detected by flow cytometry of *WT*, $Nrf1\alpha^{-/-}$ and $Nrf2^{-/-}$ cell lines that had been cultured in 25 mM or 5 mM glucose media for 24 h, and then stained by DCFH for 30 min.

(B) A schematic representation of the redox metabolic process after glucose enters the cell.

(C) Differential mRNA expression levels of *HK1, HK2, GLUT1, GLUT4, LDHA, PDH, PDK1, SREBP1, SREBP2, ACCα, ACLY, FASN, SCD1,* and *CPT1A* were determined by RT-qPCR in *WT*, $Nrf1\alpha^{-/-}$ and $Nrf2^{-/-}$ cells. The data are shown as mean ± SEM (n = 3 × 3; $, $p < 0.05$ and $$, $p < 0.01$; *, $p < 0.05$ and **, $p < 0.01$).

(D) Changed abundances of HK1, HK2, Glut1, Glut4, LDHA, PDH, SREBP1, SREBP2, FASN, SCD1, and CPT1A in *WT*, $Nrf1\alpha^{-/-}$ and $Nrf2^{-/-}$ cells were visualized by Western blotting. The immunoblotting intensity was calculated as shown on the bottom.

(E) The mRNA level of *Nrf2, GCLM, HO1, HK1, HK2, GLUT1, GLUT4, G6PD, LDHA, PDH, PDK1, SREBP1, ACCα, ACLY, FASN, SCD1,* and *CPT1A* were determined by RT-qPCR in $Nrf1\alpha^{-/-}$ cells, which had been interfered by siRNA specific targeting Nrf2 (siNrf2) or scrambled siRNA (siNC). The resulting data are shown as mean ± SEM (n = 3 × 3; *, $p < 0.05$ and **, $p < 0.01$).

(F) The protein levels of Nrf2, GCLM, HO1, HK1, HK2, Glut1, Glut4, G6PD, LDHA, PDH, SREBP1, ACCα FASN, and SCD1 were visualized by Western blotting in $Nrf1\alpha^{-/-}$ cells that were interfered by siNrf2 or siNC. The intensity of all the immunoblots was calculated as shown on the bottom.

(G) Changes in ROS levels were detected by flow cytometry of $Nrf1\alpha^{-/-}$ cells that had been interfered with by siNrf2 or siNC and cultured in 25 mM or 5 mM glucose media for 24 h and then stained by DCFH for 30 min.

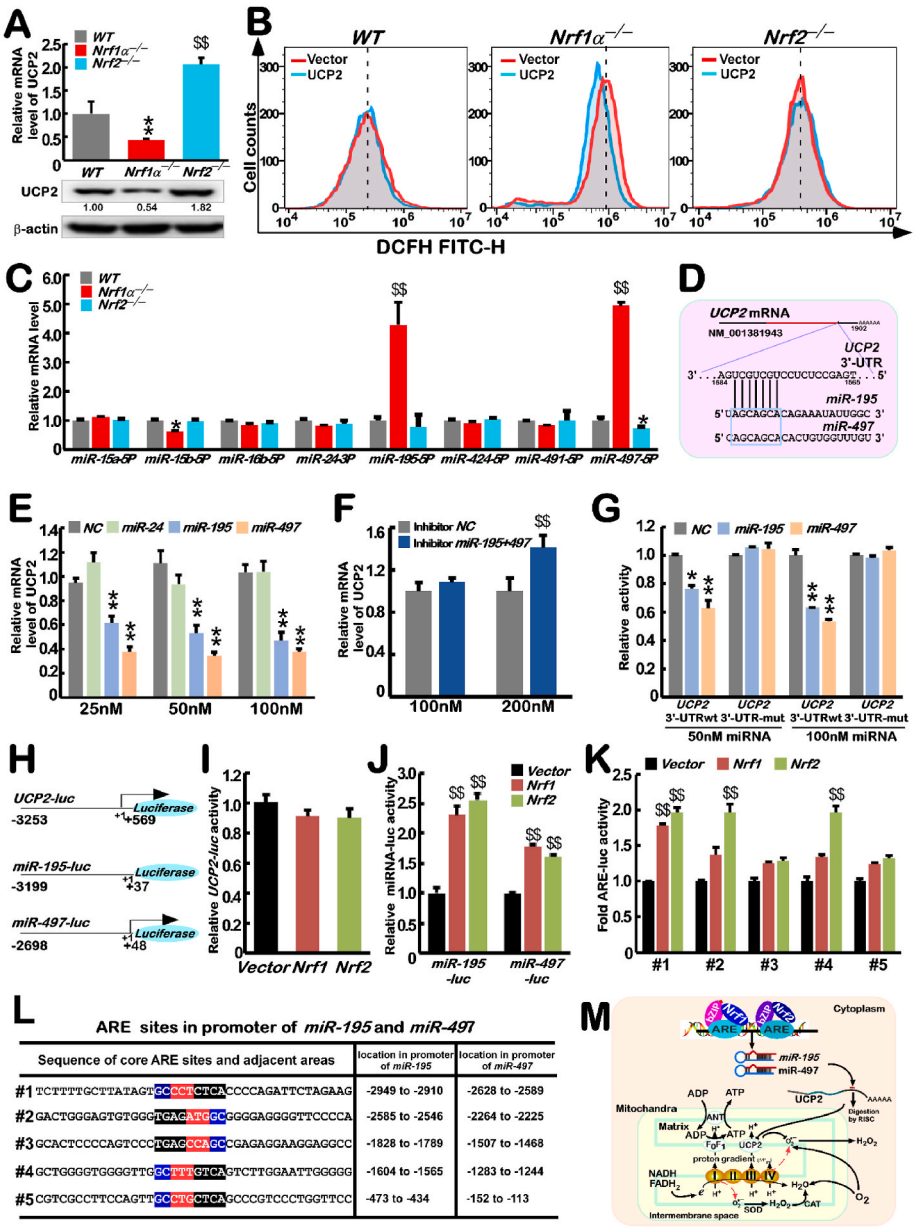

Fig. 5. Distinct effects of Nrf1 and Nrf2 on ROS production by inhibiting UCP2 *via* miRNA-195 and miRNA-497

(A) The mRNA (*upper column*) and protein (*lower panel*) levels of *UCP2* were determined by RT-qPCR and Western blotting of *WT*, *Nrf1α*$^{-/-}$ and *Nrf2*$^{-/-}$ cells. The qPCR data are shown as mean ± SEM (n = 3 × 3; $$, $p < 0.01$; **, $p < 0.01$). The intensity of all the immunoblots was calculated as shown on the bottom.

(B) *WT*, *Nrf1α*$^{-/-}$ and *Nrf2*$^{-/-}$ cell lines were allowed for the forced expression of UCP2 or empty vector, and then for 24-h recovery from transfection, before ROS levels of cells are detected by flow cytometry.

(C) Relative mRNA level of *miR-15a-5P, miR-15b-5P, miR-16b-5P, miR-24-3P, miR-195-5P, miR-424-5P, miR-491-5P,* and *miR-497-5P* in *WT*, *Nrf1α*$^{-/-}$ and *Nrf2*$^{-/-}$ cells were determined by RT-qPCR. The data are shown as mean ± SEM (n = 3 × 3; $$, $p < 0.01$; *, $p < 0.05$).

(D) Schematic representation of miR-195 and miR-497 targeting the 3'-UTR of *UCP2*.

(E) WT cells were transfected with miR-24, miR-195 or miR-497 mimics in indicated concentration, and then allowed for 24-h recovery from transfection, because the mRNA levels of *UCP2* were determined by RT-qPCR. The data are shown as fold changes (mean ± SEM, n = 3 × 3; **, $p < 0.01$).

(F) After *Nrf1α*$^{-/-}$ cells were transfected with the inhibitors of miR-195 and miR-497, the mRNA levels of *UCP2* were determined by RT-qPCR. The data are shown as mean ± SEM (n = 3 × 3; $$, $p < 0.01$).

(G) The 3'-UTR of *UCP2* were cloned into a psiCHECK-2 plasmid, and co-transfected with miR-195, miR-497, or negative controls. After 24-h recovery from transfection, the miRNA activity of binding to 3'-UTR of *UCP2* was assayed by indicated Ranilla luciferase reporters, luciferase gene in psiCHECK-2 plasmid was used as an internal reference. The data are shown as fold changes (mean ± SEM, n = 3 × 3; **, $p < 0.01$).

(H) Schematic representation of the *UCP2-luc, miR-195-luc, and miR-497-luc* reporters, which were constructed into the PGL3-Promoter plasmid. These gene promoter regions were also indicated.

(I) Relative activity of *UCP2-luc* was determined in the cells that were co-expressed with each of indicated luciferase reporters, and pRL-TK, plus an expression construct for Nrf1 or Nrf2, or empty pcDNA3 plasmid and then allowed for 24-h recovery from transfection. The resulting data are shown as mean ± SEM (n = 3 × 3).

(J) Relative activity of *miR-195-luc and miR-497-luc* were determined as described above (mean ± SEM, n = 3 × 3; $$, $p < 0.01$).

(K) Fold activity of *ARE-luc* activated by Nrf1 or Nrf2 was determined. These ARE-adjoining sequences listed in (L) were cloned into PGL3-promoter plasmid and were co-transfected with pRL-TK, plus an expression construct for Nrf1 or Nrf2, or empty pcDNA3 plasmid.

(L) Distinct locations of ARE sites from the promoters of *miR-195* and *miR-497* were listed herein.

(M) A proposed model to explain the distinct effects of Nrf1 and Nrf2 on ROS production by inhibiting UCP2 *via* miR195 and miR497.

glycolytic inhibition by 2-deoxy-D-glucose (2-DG in 25 mM glucose media) led to distinct extents of decreased ROS yield in *Nrf1α*$^{-/-}$ or *Nrf2*$^{-/-}$ cell lines (Fig. S10A), but an apparent increase of ROS in *WT* cells occurred after 2-DG treatment. However, treatment of *Nrf1α*$^{-/-}$cells with insulin (to activate glycolysis) caused a modest increase in ROS, while no changes in ROS yielded from insulin-treated *WT or Nrf2*$^{-/-}$ cell lines were determined (Figs. S10B and S10C). Collectively, these data suggest that glycolysis contributes to ROS production, especially in

Nrf1α$^{-/-}$cells, and decreased metabolism in *Nrf2*$^{-/-}$ cells could impede the yield of ROS by feeding 25 mM glucose to oxidative metabolism (e.g., glycolysis).

Those key genes involved in glucose and lipid metabolic pathways (as illustrated in Fig. 4B) were further examined herein. Both RT-qPCR and WB results showed that hexokinases (HK1 and HK2, the first rate-limiting enzymes of glycolysis to yield glucose 6 phosphate), along with glucose transporters (Glut1, and Glut4) are all highly expressed in *Nrf1α*$^{-/-}$ cells, of which HK1 and Glut4 are also obviously up-regulated in *Nrf2*$^{-/-}$ cells to considerably higher levels, but that were rather lower than those obtained in *Nrf1α*$^{-/-}$ cells (Figs. 4C and 4D). In addition, the pyruvate content in *Nrf1α*$^{-/-}$ cells was increased, while decreased in *Nrf2*$^{-/-}$ cells (Fig. S10D), this implies an enhancement of glycolysis in *Nrf1α*$^{-/-}$cells, as consistent with a previous report [20,43]. This is also evidenced by further examinations, revealing that pyruvate dehydrogenase (PDH) was modestly up-regulated in *Nrf1α*$^{-/-}$cells (with hyperactive Nrf2 accumulated), and thus down-regulated in *Nrf2*$^{-/-}$ cells (Figs. 4C and 4D). Rather, no changes in basal expression of pyruvate dehydrogenase kinase 1 (PDK1, as a specific inhibitor of PDH) and lactate dehydrogenase A (LDHA) were observed in these experimental cells (Figs. 4C and 4D). Such being the conditions, this facilitates the fuel loading by glycolysis insomuch as to enter the mitochondria, leading to an increased pressure on the oxidative respiratory chain to produce the excessive ROS in this organelles of *Nrf1α*$^{-/-}$cells. Furthermore, it was also found that other critical genes *SREBP1, SREBP2, ACLY* (ATP citrate lyase)*, ACCα* (Acetyl-CoA Carboxylase Alpha)*, FASN* (fatty acid synthase) and *SCD1* (stearoyl-CoA desaturase 1) (all responsible for fatty acid synthesis) were significantly up-regulated in *Nrf1α*$^{-/-}$cells, but rather down-regulated in *Nrf2*$^{-/-}$ cells (Figs. 4C and 4D). In addition, the triglyceride content in *Nrf1α*$^{-/-}$ cells was increased (Fig. S10E), this implies that loss of *Nrf1α* rather than *Nrf2* results in an increase in fatty acid synthesis, providing a material basis for the proliferation of *Nrf1α*$^{-/-}$cells. Also, such increased synthesis of fatty acids has to consume a certain amount of NADPH generated by the pentose phosphate pathway and hence leads to a decrease in the antioxidant capability of the cell. Conversely, this appears to be supported by Scheffler's group, demonstrating that a genetic respiratory chain deficiency could block the TCA cycle [44], serving as a vital hub towards *de novo* lipid synthesis (as illustrated in Fig. 4B). Thereby, it is inferable that the elevated lipid synthesis is considered an important outlet for glycolytic flux in *Nrf1α*$^{-/-}$cells, as accompanied by its mitochondrial oxidative damages.

Since Nrf2 is aberrantly accumulated in *Nrf1α*$^{-/-}$cells as aforementioned, the role of Nrf2 in this metabolic process was investigated by specific siRNAs interfering with Nrf2. As shown in Figs. 4E & 4F, significant decreases in mRNA and protein expression of Nrf2 and target genes *HO1* and *GCLM* were caused by the silencing of Nrf2 in *Nrf1α*$^{-/-}$cells. In the meanwhile, all other examined genes except PDH and PDK (involved in glucose and lipid metabolism) are also down-regulated by knockdown of Nrf2 to varying degrees (Figs. 4E and 4F). Among them, HK2, Glut1, Glut4, G6PD, ACCα, ACLY, FASN and SCD1 were substantially inhibited by interfering Nrf2 (Figs. 4E and 4F). Further studies unraveled that such knockdown of Nrf2 in *Nrf1α*$^{-/-}$cells did not reverse but shortened the reduced ROS led by 5 mM glucose (Fig. 4G), with the apoptosis unchanged (Fig. S11A). In addition, knockdown of Nrf2 in *Nrf1α*$^{-/-}$cells led to an increase in the intracellular ROS and apoptosis, when compared to equivalent controls (Fig. S11B), implying an antioxidant cytoprotective role of Nrf2 against oxidative damages. Altogether, loss of Nrf1α may stimulate a surge of Nrf2 accumulated to enhance glycolysis and lipid synthesis; this is also accompanied by increased pressure of the *Nrf1α*$^{-/-}$-damaged mitochondria to generate the excessive ROS. In turn, the elimination of ROS by the Nrf2-mediated antioxidant cytoprotective mechanism is also reinforced. Therefore, it is postulated that Nrf2 may provide a decisive interplay to balance between ROS arising from cellular metabolism and antioxidant response.

3.5. Mitochondrial UCP2 is negatively regulated by Nrf2 via miR-195 and miR-497 to augment ROS, even in *Nrf1α*$^{-/-}$ cells

Besides the glycolytic flux entering the mitochondria, its uncoupling proteins (UCPs) can also monitor the production of ROS in these organelles [45]. Among them, UCP1 was reported to be positively correlated with Nrf1, but it is dominantly expressed in white adipose tissue [46], while UCP2 is widely expressed in various tissues, though they can reduce the mitochondrial $\Delta\psi_m$ by 'mild uncoupling' insomuch as to negatively regulate the yield of ROS [45,47]. Here, our evidence revealed that basal mRNA and protein levels of *UCP2* were significantly decreased in *Nrf1α*$^{-/-}$cells, but up-expressed to considerably higher extents in *Nrf2*$^{-/-}$cells when compared to *WT* controls (Fig. 5A). Next, we examined the effect of UCP2 on the production of ROS by forced expression of UCP2 in distinct genotypic cell lines (Figs. 5B and S12A). The results unraveled that the ROS levels in *Nrf1α*$^{-/-}$cells (with hyperactive Nrf2) were significantly decreased by over-expression of UCP2, but almost unaffected in *Nrf2*$^{-/-}$ and *WT* cell lines (Fig. 5B). Collectively, these indicate that Nrf2 may exert a dominant inhibitory effect on UCP2 to promote the yield of ROS in *Nrf1α*$^{-/-}$cells.

To gain insight into the putative inhibitory effect of Nrf2 on UCP2, we further investigated this gene promotor and its mRNA regulatory mechanisms, As shown in Fig. 5C, among eight candidate miRNAs for targeting 3'-UTR of *UCP2*'s mRNA predicated by online databases (http://www.targetscan.org/ and http://ophid.utoronto.ca/mirDIP/index.jsp#r), only miR-195 and miR-497 were highly expressed in *Nrf1α*$^{-/-}$cells, but unaltered or even down-regulated, respectively, in *Nrf2*$^{-/-}$cells, just as opposed to basal expression of UCP2 (Fig. 5A). The sequence analysis of miR-195 and miR-497 deciphered a conserved homology targeting their complementary 7-nucleotide motif within 3'-UTR of UCP2 (Fig. 5D). As anticipated, the results from RT-qPCR revealed that the mRNA expression levels of UCP2 were effectively down-regulated by transfecting different concentrations of miR-195 or miR-497, but not miR-24, into *WT* cells (Fig. 5E). In the parallel experiments, the decreased expression of *UCP2* in *Nrf1α*$^{-/-}$cells was restored by a co-inhibitor of both miR-195 and miR-497 (Fig. 5F).

To validate the putative interaction of either miR-195 or miR-497 with *UCP2* mRNA, we cloned their 3'-UTR or mutants into a luciferase reporter vector before being co-transfected into *WT* cells. As expected, the results demonstrated that the 3'-UTR-driven reporter activity was inhibited by miR-195 or miR-497, but such inhibitory effects were sufficiently abrogated by its mutants from 3'-UTR of *UCP2* mRNA (Fig. 5G). Next, we constructed three reporter genes by cloning distinct lengths of the examined promoter regions of *UCP2*, *miR-195* and *miR-497* (i.e., *UCP2-Luc*, *miR-195-Luc,* and *miR-497-Luc*, Fig. 5H), to verify whether they are regulated by Nrf1 and/or Nrf2. The luciferase assays showed that the *UCP2-Luc* transcriptional activity was almost unaffected by Nrf1 or Nrf2 (Fig. 5I). However, transactivation activity of *miR-195-Luc* or *miR-497-Luc* reporters was significantly induced by co-transfection with Nrf1 or Nrf2 (Fig. 5J). Further analysis of the promoter regions of *miR-195* and *miR-497* uncovered that their promoters are almost completely overlapped and comprise five common *ARE* consensus sites (Fig. 5K). Among these ARE-driven luciferase reporters made by ligating the indicated sequences into the PGL3-promoter vector, only #1 transactivation activity was modestly mediated by Nrf1, while Nrf2 enabled to mediate significant induction of #1, #2 and #4 reporters (Fig. 5L). However, ChIP-sequencing data obtained from the Encode database failed to show significant peaks of both Nrf1 and Nrf2 activities to binding multiple ARE sites within the promoter regions of *miR-195* and *miR-497* (Fig. S12B). As such, taking all available data into consideration, we propose that Nrf2 (and Nrf1) possess a capability to down-regulate the *UCP2* gene activity indirectly by cognate ARE-driven expression of miR-195 and/or miR-497 (Fig 5M). This notion is also further supported by additional evidence that a remarkable decrease of *UCP2* at its mRNA and protein expression levels occurred upon tetracycline-inducible expression of either Nrf1 or Nrf2 in HEK293 cells

(Fig. S12C).

3.6. Loss of Nrf1α leads to inactivation of the mitochondrial stress response, albeit Nrf2 is hyperactive, in Nrf1α$^{-/-}$ cells

To maintain mitochondrial homeostasis, all eukaryotic cells have evolutionarily developed a nuclearly-controlled transcriptional responsive programme, called mitochondrial unfolded protein response (UPR^{mt}) [48]. If it is required for mitochondrial functioning, UPR^{mt} is triggered to actively promote the repair and recovery of mitochondrial function and integrity. In *Caenorhabditis elegans,* the UPR^{mt} is monitored primarily by the stress-activated transcription factor ATFS-1 (of the basic-region leucine zipper family), as well by SKN-1 (skinhead-1, sharing an orthologous homology with Nrf1 and Nrf2) [49,50]. The mammalian UPR^{mt} is regulated by ATF5 (activating transcription factor 5)-mediated expression of several mitochondrial chaperones and protease genes to promote its OXPHOS and cell growth during mitochondrial dysfunction [51]. Besides, ATF4 (activating transcription factor 4) and CHOP are also involved in the activation of UPR^{mt} [52,53]. Our previous study has found that loss of Nrf1 results in down-regulation of ER-stress-related genes (Figs. S13A and S13B) [54]. Herein, our evidence revealed that basal expression of *ATF5*, *ATF4* and *CHOP*, along with their targets *HSP60* (60 KDa heat shock protein, mitochondrial), *GRP75* (i.e. *mtHSP70, stress-70 protein, mitochondrial*), and *FGF21* (fibroblast growth factor 21) was, to different degrees, lowered in *Nrf1α*$^{-/-}$cells (Fig. S13B). Of note, these two key chaperones HSP60 and GRP75 are controlled by ATF5 in folding the denatured and nascent polypeptides in the mitochondria, while FGF21 is regulated by ATF4 in metabolic adaptation to fasting [55]. By contrast with *Nrf1α*$^{-/-}$cells, putative inactivation of UPR^{mt} did not appear to occur in *Nrf2*$^{-/-}$cells when compared with a similar status of *WT* cells (Fig. S13B).

To determine the effect of Nrf1 or Nrf2 deficiency on UPR^{mt}, *Nrf1α*$^{-/-}$ and *Nrf2*$^{-/-}$cell lines were treated with carbonyl cyanide-p-trifluoromethoxyphenylhydrazone (FCCP, an uncoupling reagent to disrupt ATP synthesis by transporting H^+ ion through the mitochondrial membrane before being used for oxidative phosphorylation, thus to activate UPR^{mt} as reported by Refs. [53,56–58]). The results unraveled that *Nrf1* and *Nrf2* at the mRNA and protein levels were induced by FCCP in *WT* cells (Figs. 6A and 6B). Albeit transcriptional expression of Nrf1 was reportedly regulated by Nrf2 [29], it was still stimulated by FCCP in *Nrf2*$^{-/-}$cells. Conversely, mRNA expression levels of Nrf2 were unaffected by FCCP in *Nrf1α*$^{-/-}$ cells, even though its protein appeared to

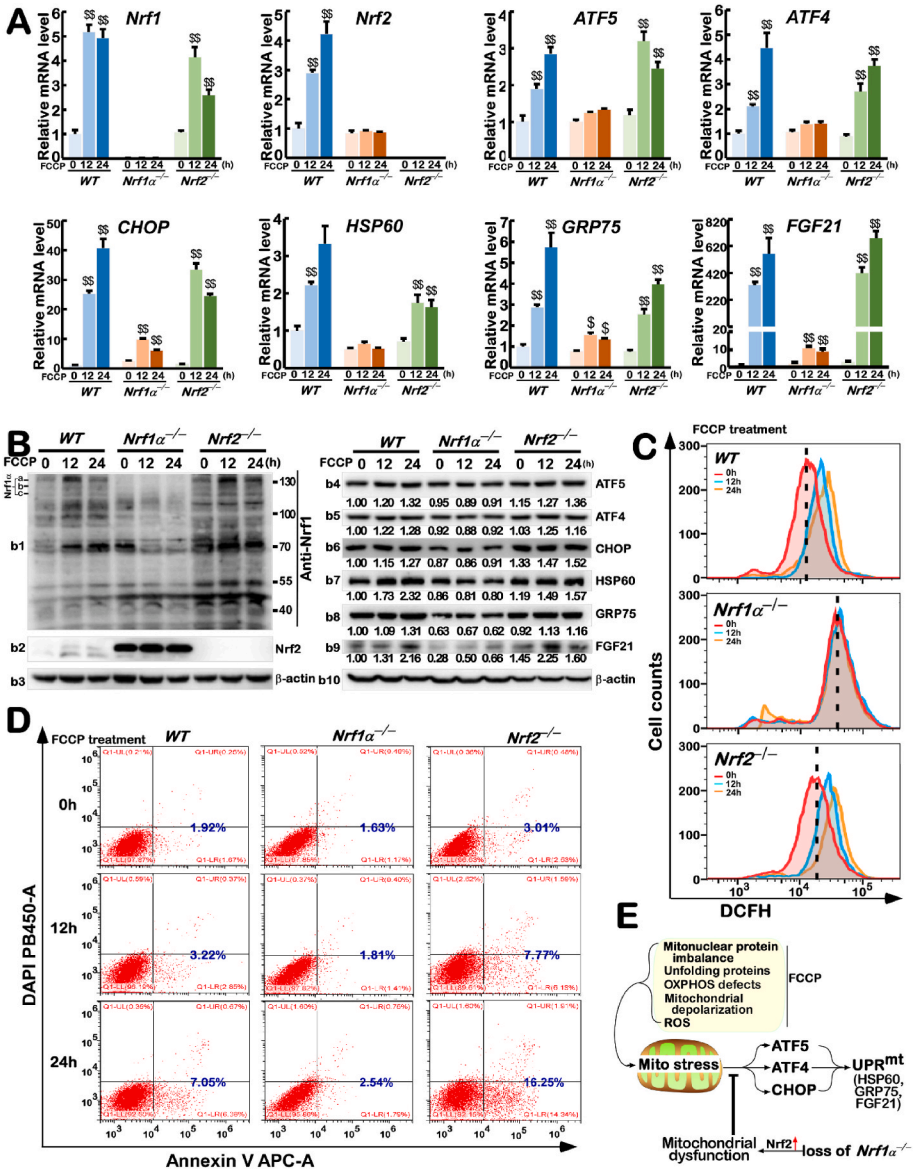

Fig. 6. Nrf1 is essentially required for activation of mitochondrial stress-related responsive genes

(A) The mRNA levels of *Nrf1, Nrf2, ATF5, ATF4, CHOP, HSP60, GRP75,* and *FGF21* were determined by RT-qPCR in *WT*, *Nrf1α*$^{-/-}$ and *Nrf2*$^{-/-}$ cells, which had been treated with FCCP for 0 h, 12 h or 24 h. The data are shown as mean ± SEM (n = 3 × 3) with significant increases ($, $p < 0.05$ and $$, $p < 0.01$) as compared to the untreated cases.

(B) The protein levels of indicated genes above were visualized by Western blotting in *WT*, *Nrf1α*$^{-/-}$ and *Nrf2*$^{-/-}$ cells, which had been treated with FCCP for 0 h, 12 h, or 24 h. The intensity of all the immunoblots was calculated as shown on the bottom.

(C) Changes in ROS levels were detected by flow cytometry in *WT*, *Nrf1α*$^{-/-}$ and *Nrf2*$^{-/-}$ cells that had been treated by FCCP for 0 h, 12 h, or 24 h, and then stained by DCFH for 30 min.

(D) The apoptosis was analyzed by flow cytometry in *WT*, *Nrf1α*$^{-/-}$ and *Nrf2*$^{-/-}$ cells, after they had been treated by FCCP for 0 h, 12 h, or 24 h and then incubated with Annexin V-FITC and PI.

(E) A proposed model to explain an essential role of Nrf1 in mediating mitochondria unfolded protein response.

be further accumulated (Figs. 6A and 6B). Further examinations revealed that FCCP-inducible expression levels of *ATF4*, *ATF5*, *CHOP*, *HSP60*, *GRP75* and *FGF21* were almost completely abolished in *Nrf1α*$^{-/-}$ cells, but not or less altered in *Nrf2*$^{-/-}$cells than those obtained from *WT* cells (Figs. 6A & 6C). Collectively, these demonstrate that Nrf1, rather than Nrf2, is a dominant activator involved essentially in the FCCP-induced UPR^{mt}.

Further treatment of *WT* cells with FCCP caused a significant increment in the production of ROS in a time-dependent manner (Fig. 6D); this was also accompanied by increased apoptosis (Fig. 6E). In sharp contrast, FCCP-caused ROS and apoptosis were substantially augmented in *Nrf2*$^{-/-}$cells (Fig. 6D and 6E). However, it is, much to our surprise, found that almost no changes in the intracellular ROS levels and apoptosis of *Nrf1α*$^{-/-}$ cells occurred after treatment of FCCP (Figs. 6D and 6E). This implies that no proper UPR^{mt} to FCCP is instigated in the dysfunctional mitochondria caused by loss of Nrf1α, although hyperactive Nrf2 is retained in *Nrf1α*$^{-/-}$ cells (Fig. 6F). Conversely, loss of Nrf2 may render its deficient cells to rely much on the energy supply of mitochondria.

3.7. The EMT-relevant signaling pathways are constitutively activated in *Nrf1α*$^{-/-}$ cells

The above-described evidence revealed that mildly increased ROS in *Nrf2*$^{-/-}$cells is attributable to the diminishment of the antioxidant capability to scavenge ROS, while *Nrf1α*$^{-/-}$ cells give rise to a severe amount of ROS in impaired mitochondria, possibly leading to malignant cell proliferation as reported previously [29]. Herein, to further determine the underlying mechanisms by which loss-of-function of Nrf1α enables to serve an original impact on tumorigenesis and development, we examined several discrete signaling pathways provoked by ROS, which are all converged on the EMT-relevant process involved in carcinogenesis and malignance (including invasion and migration). As illustrated in Fig. 7A, the migrating ability of *Nrf1α*$^{-/-}$ cells through transwells was greatly enhanced, while the migration of *Nrf2*$^{-/-}$cells became rather weakened, when compared to that of *WT* cells. Further examinations revealed that the epithelial marker proteins CDH1 (E-cadherin) were down-regulated in *Nrf1α*$^{-/-}$ cells, but the mesenchymal marker proteins CDH2 (N-cadherin), vimentin and FN1 (fibronectin 1) were up-regulated in this deficient cells (Fig. 7B, *b1 to b4*). Conversely, in *Nrf2*$^{-/-}$cells, CDH1 was substantially incremented, while

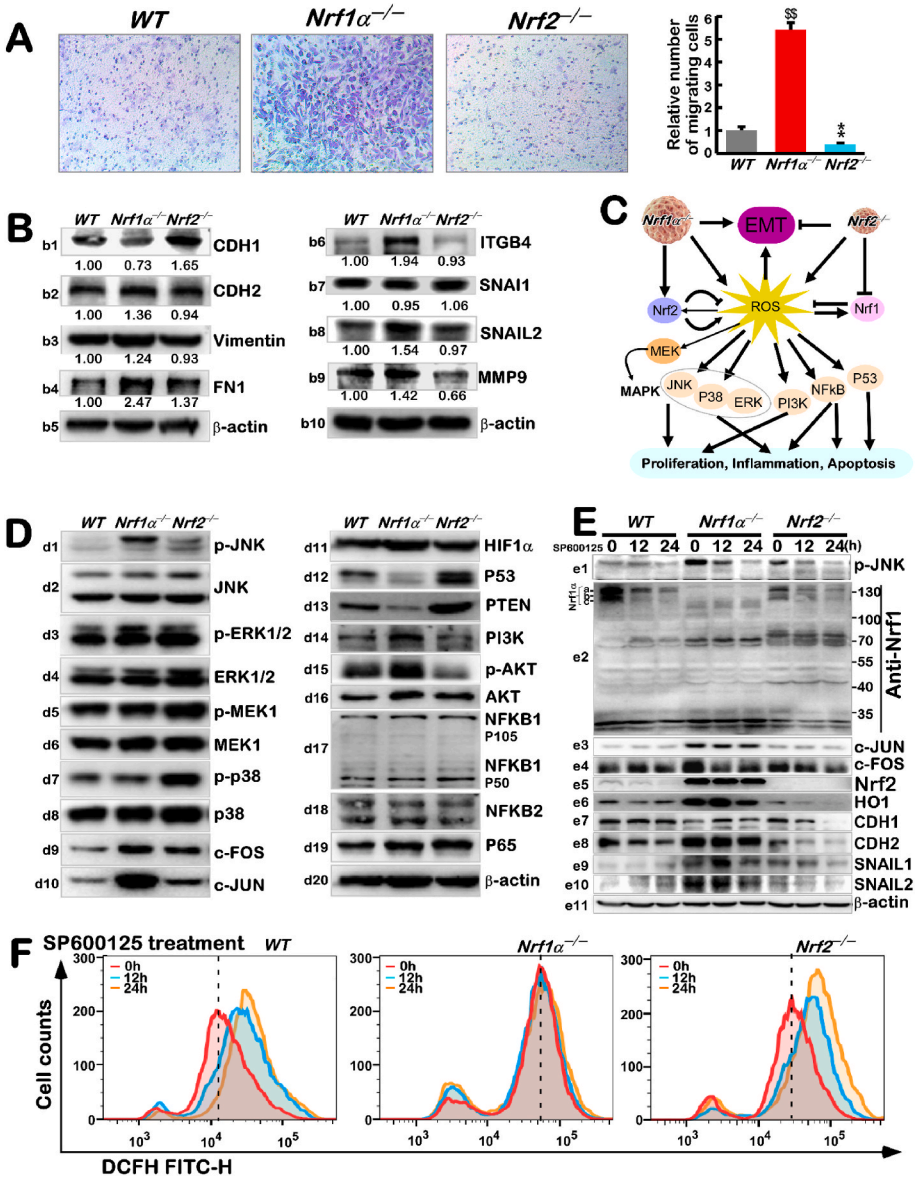

Fig. 7. Distinctive effects of *Nrf1α*$^{-/-}$ and *Nrf2*$^{-/-}$ on EMT-related genes and ROS-triggered signaling pathways

(A) *WT*, *Nrf1α*$^{-/-}$ and *Nrf2*$^{-/-}$ cells were starved for 12 h in a serum-free medium and subjected to transwell migration before being Captured by microscope. Counts of migrated cells are shown as fold changes in right panel (mean ± SEM, n = 3 × 3; $$, $p < 0.01$; **, $p < 0.01$).

(B) The protein levels of CDH1, CDH2, Vimentin, FN1, ITGB4, SNAI1, SNAIL2, MMP9, and P53 were visualized by Western blotting in *WT*, *Nrf1α*$^{-/-}$ and *Nrf2*$^{-/-}$ cells. The intensity of all the immunoblots was calculated as shown on the bottom.

(C) A schematic representation of EMT and ROS-triggered signaling pathways.

(D) Abundances of p-JNK, JNK, p-ERK1/2, ERK1/2, p-MEK1, MEK, p-p38, p38, HIF1α, PTEN, PI3K, p-AKT, NF-κB 2, NF-κB 1 (p105/p50), P65, and c-FOS, c-JUN proteins were visualized by Western blotting in *WT*, *Nrf1α*$^{-/-}$ and *Nrf2*$^{-/-}$ cells. The intensity of all the immunoblots was calculated and shown in Fig. S14.

(E) The protein levels of p-JNK, Nrf1, c-JUN, c-FOS, Nrf2, HO1, CDH, and SNAIL were visualized by Western blotting in *WT*, *Nrf1α*$^{-/-}$ and *Nrf2*$^{-/-}$ cells, which had been treated with SP600125 for 0 h, 12 h or 24 h.

(F) ROS levels were detected by flow cytometry in *WT*, *Nrf1α*$^{-/-}$ and *Nrf2*$^{-/-}$ cells, which had been treated by SP600125 for 0 h, 12 h, or 24 h, and then stained by DCFH for 30 min.

CDH2 and FN1 were roughly unaltered. Interestingly, ITGB4 (integrin subunit beta 4, a key node making the cell-cell interaction and communication with the extracellular matrix) was markedly increased in *Nrf1α*$^{-/-}$ cells but rather diminished in *Nrf2*$^{-/-}$cells (Fig. 7B, *b6*). Aside from SNAI1 (snail family transcriptional repressor 1) which was unaffected in these two deficient cell lines, SNAIL2 (snail family transcriptional repressor 2) was significantly augmented in *Nrf1α*$^{-/-}$ cells, but was unchanged in *Nrf2*$^{-/-}$cells (Fig. 7B, *b7 & b8*), albeit both factors were shown to activate the EMT-relevant transcriptional programme during liver fibrosis and cancer development, but also repress the epithelial genes by binding to their E-box DNA sequences [59]. In addition, MMP9 (matrix metallopeptidase 9, which can enhance the extracellular matrix protein degradation and hence enable invasion) was up-regulated in *Nrf1α*$^{-/-}$ cells, but down-regulated in *Nrf2*$^{-/-}$cells (Fig. 7B, *b9*). Taken altogether, these demonstrate that loss of Nrf1α leads to promotion of the EMT and malignant behavior, but such effects appear to be suppressed by loss of Nrf2, although its ROS levels were also increased.

Such discrepant consequences in the migration of between *Nrf1α*$^{-/-}$ and *Nrf2*$^{-/-}$cell lines, although both have given rise to evident increases in their intracellular ROS levels, suggest that distinct signaling pathways are likely to be activated by different extents of ROS-caused redox stress in the two distinctive genotypic cell lines (Fig. 3C). Firstly, examinations of the expression of mitogen-activated protein kinases (MAPKs, including ERKs, JNK and p38 kinase, that play key roles in tissue homeostasis, cell proliferation, differentiation survival and migration, as well in inflammation and carcinogenesis [60]) unraveled that phosphorylated abundance of JNK was substantially augmented in *Nrf1α*$^{-/-}$ cells, but only modestly increased in *Nrf2*$^{-/-}$cells, albeit its total protein expression levels were slightly enhanced in the two cell lines (Fig. 7D, *d1 & d2*). Conversely, the phosphorylated ERKs and p38, as well as their upstream kinase MEK were strikingly elevated in *Nrf2*$^{-/-}$cells, but almost unchanged in *Nrf1α*$^{-/-}$ cells (Fig. 7D, *d3 to d8*). Their downstream c-JUN and c-FOS (two key constituents of AP1 involved in tumorigenesis) were markedly up-regulated in both *Nrf1α*$^{-/-}$ and *Nrf2*$^{-/-}$cell lines (Fig. 7D, *d9 & d10*). Such increased c-JUN abundance was nearly 6 folds, while the increased c-FOS was also nearly 4 folds in *Nrf1α*$^{-/-}$ cells, but both proteins were about 2 folds in *Nrf2*$^{-/-}$cells, as compared to *WT* controls (Fig. S14). Thereafter, it was found that HIF1α (a critical factor for hypoxic stress response) was increased in *Nrf1α*$^{-/-}$ cells, but almost unaffected in *Nrf2*$^{-/-}$cells (Fig. 7D, *d11*). However, the versatile p53 expression was almost abrogated in *Nrf1α*$^{-/-}$ cells but significantly up-regulated in *Nrf2*$^{-/-}$cells (Fig. 7D, *d12*).

Next, basal expression of key signal molecules involving the PTEN-

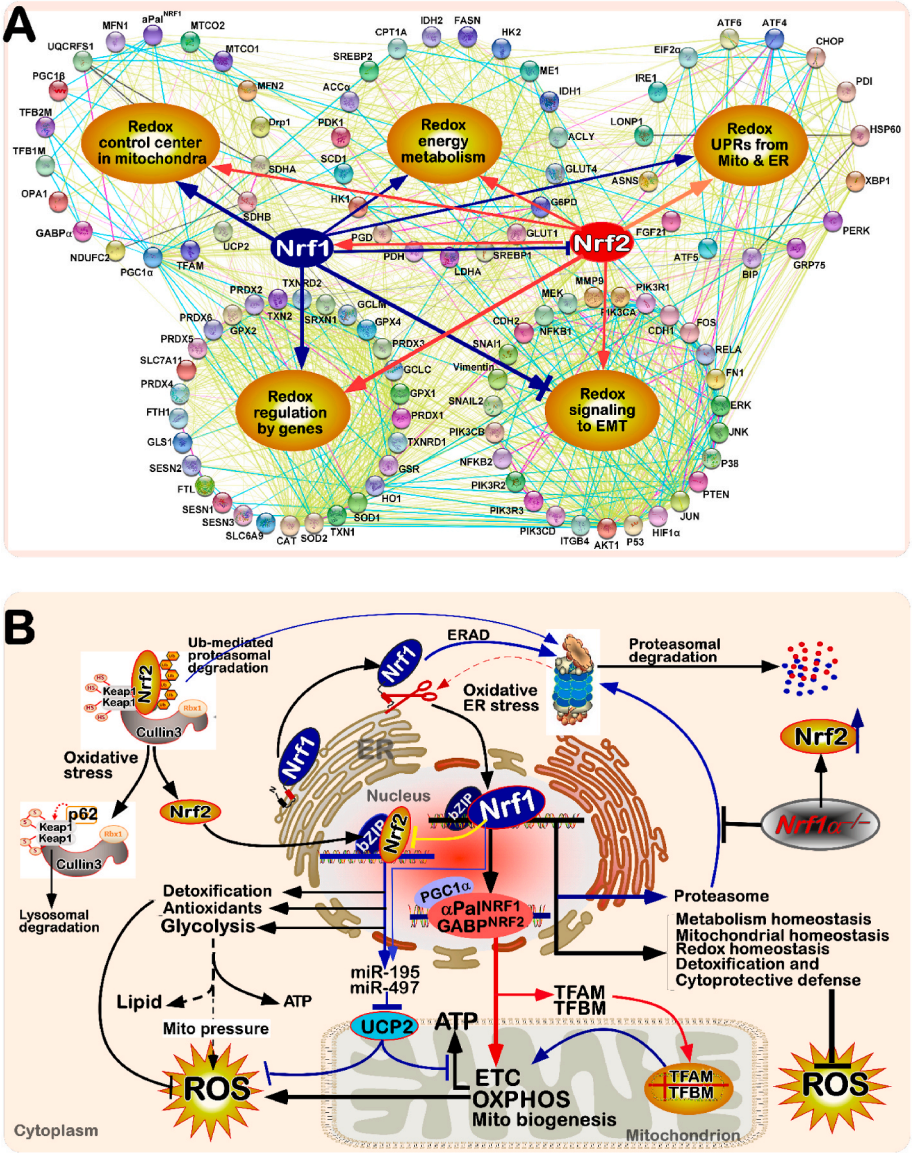

Fig. 8. Distinct roles of Nrf1 and Nrf2 in nuclearly-controlled mitochondrial functional networks.
(A) A multi-hierarchical regulatory network monitored by Nrf1 and Nrf2 alone or together. Those protein-protein associations are determined in various ways, and thus represented by different colored edges as indicated.
(B) A comprehensive regulatory model is proposed to explain an indispensable function of Nrf1 as a redox-determining factor for mitochondrial homeostasis.

PI3K-AKT and NF-κB pathways were examined, albeit a previous study showed that PTEN (a potent tumor suppressor, that negatively regulates the PI3K-AKT signaling to inhibit cell proliferation and survival [61]) is blocked by ROS-induced Nrf2 through miR-22 [29]. Herein, basal PTEN expression was almost completely abolished in *Nrf1α*$^{-/-}$ cells, but conversely remarkably increased in *Nrf2*$^{-/-}$cells (Fig. 7D, *d13*). Accordingly, both phosphorylated proteins of PI3K (p110) and AKT were significantly up-regulated in *Nrf1α*$^{-/-}$ cells, but rather down-regulated in *Nrf2*$^{-/-}$cells (Fig. 7D, *d14* to *d15*). This finding provides a better understanding of the malignant proliferation of tumors occurring upon loss of Nrf1α. Furthermore, only the p65 subunit of NF-κB (as a key factor responsible for the inflammatory response to ROS) was only modestly up-regulated in both *Nrf1α*$^{-/-}$ and *Nrf2*$^{-/-}$cell lines (Fig. 7D, *d19*), but the other relevant NF-κB1 and NF-κB2 were unchanged (Fig. 7D, *d17 & d18*).

Lastly, treatments of *WT* cells with a JNK-specific inhibitor SP600125 revealed that Nrf1, Nrf2 and all relevant target genes were suppressed significantly (Fig. 7E). Similar inhibitory effects were also exerted in *Nrf2*$^{-/-}$cells. By contrast, although auto-phosphorylated JNK, along with c-JUN and c-FOS in *Nrf1α*$^{-/-}$ cells were strikingly prevented by SP600125 (Fig. 7E), Nrf2, CDH1 and CDH2 were largely unaffected by SP600125, while HO1, SNAIL1 and SNAIL1 were partially altered (*e5 to e10*). This implies they may be also modulated independently of the JNK-AP1 signaling, particularly in *Nrf1α*$^{-/-}$ cells. Intriguingly, inhibition of JNK caused a sharp increment in intracellular ROS in *WT* and *Nrf2*$^{-/-}$cells, but nearly unchanged in *Nrf1α*$^{-/-}$ cells (Fig. 7F), reflecting a crucial cytoprotective role of JNK and AP1 in the response to oxidative stress. Overall, loss of *Nrf1α*$^{-/-}$ or *Nrf2*$^{-/-}$ leads to differential dysregulation of multi-hierarchical signaling pathways to cognate target gene networks at distinct layers, by varying extents of their endogenous oxidative stress during different cell processes (Fig. 8).

4. Discussion

Just because ROS has a 'double-edged sword' effect with dual characteristics of beneficial hormesis and harmful cytotoxicity to all living cells, a steady state of redox homeostasis is robustly maintained by balancing ROS production (primarily in mitochondria) and elimination by a set of antioxidant responses and detoxification protective systems. Such a certain homeodynamic range of redox threshold should be tightly controlled by redox signaling to gene regulatory networks predominantly mediated by Nrf1 and Nrf2. Despite earlier discovery of antioxidant Nrf1 than Nrf2, less is known about Nrf1 relatively to Nrf2 albeit the highly conserved Nrf1 rather than Nrf2 is essential for redox homeostasis. This is owing to the fact that abundance of Nrf2 is monitored by Keap1 as a redox sensor, enabling Nrf2 to sensitively respond to changes in intracellular redox state, whereas Nrf1 as a membrane protein seems to relatively hardly respond to the changing redox levels. However, in addition to regulation of antioxidant genes by Nrf1 that has been confirmed, the sensitivity of Nrf1 to proteasome inhibition and cholesterol changes enables it to play a pivotal role in connecting basic antioxidants to other biological processes. In this study, we have provided a brand-new view of distinct roles for Nrf1 and Nrf2 played in redox regulation by distinctive mechanisms.

4.1. Distinct roles of Nrf1 and Nrf2 in redox regulation

Herein, we found that loss of either Nrf1 or Nrf2 leads to a redox imbalance to increased levels of intracellular ROS, which occurs by distinct rational mechanisms. This is because knockout of Nrf2 results in a reduction of its cellular capability to eliminate ROS insomuch as to make a redox bias towards yield of ROS. In sharp contrast, a similar capability to eliminate ROS appears to be undiminished by the knockout of Nrf1, but conversely, the production of ROS in the mitochondria is increased strikingly in *Nrf1α*$^{-/-}$ cells. Consequently, Nrf2 is accumulated in *Nrf1α*$^{-/-}$-deficient cells by its proteasomal dysfunction and further activated by increased ROS, leading to an evident enhancement of antioxidant, detoxifying and cytoprotective systems. In turn, the activity of Nrf1 appears to be not further reinforced by elevated ROS in *Nrf2*$^{-/-}$ cells. This implies that Nrf1 acts as a key constitutive transcription factor of redox regulation, but it is activated predominantly by another main way rather than ROS, or the ROS activation of Nrf1 is dependent on Nrf2. Coincidently, this is also fully consistent with our previous finding that Nrf2 serves as an upstream regulator to activate the transcriptional expression of Nrf1 [29]. Of note, as an ER-anchored membrane protein, Nrf1 is *de facto* regulated by ER-derived unfolded proteins and/or other metabolic stressors [9], to coordinate the ER homeostasis with redox homeostasis (Fig. 8), but this is required for further experiments to be elucidated.

With an aberrant accumulation of hyperactive Nrf2 in *Nrf1α*$^{-/-}$ cells, most of the antioxidant and detoxifying enzymes, as well as relevant genes responsible for the elimination of ROS are markedly augmented. Many of these up-expressed genes (e.g., encoding PRDX5, PRDX6, GPX1, SOD2, SESN2, G6PD, GCLC, GCLM, GLS1, GSR, SLC6A9, FTH1, HO1, TXN1, and TXN2) are diminished or abolished by knockout of *Nrf2*$^{-/-}$, indicating they are mainly regulated by Nrf2. Also, it cannot be ruled out that some genes are, to certain lesser extents, regulated by Nrf1, but its overlapping effects are much more likely to be concealed by hyperactive Nrf2. For example, SRXN1 and PGD were reportedly regulated by Nrf2 [62,63], and thus down-regulated in *Nrf2*$^{-/-}$ cells, but largely unchanged in *Nrf1α*$^{-/-}$ cells, implying both are co-regulated by Nrf1 and Nrf2, but the regulatory effect of Nrf1 is postulated to be offset by hyperactive Nrf2. Conversely, SESN3 was down-regulated in *Nrf1α*$^{-/-}$ cells, but almost completely abrogated in *Nrf2*$^{-/-}$ cells, implying that this putative effect of Nrf1 on SESN3 was only partially counteracted by accumulated Nrf2. In addition, PRDX4, SESN1 and TIGAR are elevated in both *Nrf1α*$^{-/-}$ and *Nrf2*$^{-/-}$ cell lines, suggesting they may be over-stimulated by elevated ROS.

4.2. Nrf1 serves as an indispensable redox-determining factor in the mitochondrial homeostasis

Albeit two independent groups had presumed that the loss of Nrf1 is likely to cause an impairment of mitochondrial functioning [23,46], no further experimental evidence has been provided in the current literature. Another group led by Yoon reported that Nrf1 acts as one of the most responsive genes when the mitochondrial respiratory chain is damaged [64,65]. In addition, a recent study also showed that interfering with Nrf1 in HepG2 cells caused mitochondrial changes and affected metabolic reprogramming [43]. These putative effects of Nrf1 prompt us to gain insights into its redox regulation for mitochondrial homeostasis because this organelle is the main resource of intracellular ROS production. The experimental evidence has been presented here, revealing that a dramatic increase of the mitochondrial ROS levels was manifested in *Nrf1α*$^{-/-}$ cells, simultaneously accompanied by significant down-regulation of key mitochondrial complex subunits upon loss of its function. However, no further increases or even modest decreases in the yield of ROS were observed after *Nrf1α*$^{-/-}$ cells had been treated with either the mitochondrial respiratory chain inhibitor rotenone or another uncoupling agent FCCP. Such dysfunctional mitochondria in *Nrf1α*$^{-/-}$ cells were damaged as evidenced by further electroscopic observations. We also observed that ROS levels in *Nrf1α*$^{-/-}$ cells decreased after rotenone treatment, presumably because rotenone blocks electrons being transferred to complex I from complex II via coenzyme Q, thereby reducing generation of ROS, which also indicates high electron transport stress on mitochondrial complex I in *Nrf1α*$^{-/-}$ cells. As such, Nrf2 is also inferred to be partially involved in mitochondrial redox stress response, because rotenone treatment of *Nrf2*$^{-/-}$ cells only modestly increased ROS generation to certain extents that are not higher than *WT* controls, meanwhile the reduction of glycolysis caused by Nrf2 knockout also reduces mitochondrial fuel loading. But, remarkable changes in its ROS occurred after FCCP treatment of *Nrf2*$^{-/-}$ cells, implying that Nrf1

remains to be expressed to a considerably high degree in *Nrf2*$^{-/-}$ cells so that deregulated mitochondria were further stressed by FCCP insomuch as to trigger excessive ROS products. In addition, it should also be noted that the basal metabolism of *Nrf2*$^{-/-}$ cells is likely placed at a rather lower level, so to enable these deficient lines to make more resistance to glucose starvation, as reported previously [35].

It is of crucial importance to discover that loss of Nrf1α results in a defective down-regulation or even abolishment of the nuclearly-controlled mitochondrial respiratory factors involving the PGC1α-αPal^{NRF1} and PGC1α-GABPα^{NRF2} pathways in *Nrf1α*$^{-/-}$ cells. Of note, PGC1α is a key transcriptional coactivator enabling for activation of estrogen-related receptors, peroxisome proliferator-activated receptors (PPARs), and other specific partners, in addition to two nuclear respiratory factors αPal^{NRF1}and GABPα^{NRF2} (Figs. 3I and 8B). Co-activation of nuclear respiratory factors αPal^{NRF1}and GABPα^{NRF2} by PGC1α further induces the expression of mitochondrially-specific transcriptional factors TFAM and TFBM, which can bind directly to both strands of mtDNA and thus play key roles in the mtDNA replication, transcription and maintenance [66]. In addition to regulating the expression of these mitochondrially-located genes through TFAM and/or TFBM, two nuclear respiratory factors αPal^{NRF1}and GABPα^{NRF2} also directly activate those nuclearly-located genes involved in the oxidative respiratory chain and mitochondrial biogenesis. Herein, our experimental evidence has unraveled that overexpression of Nrf1 and Nrf2 activates the transcriptional expression of αPal^{NRF1}, GABPα^{NRF2} and PGC1α, as well as respiratory chain subunits and that they also exert transcriptional activation effects on each of αPal^{NRF1}, GABPα^{NRF2} and PGC1α promoter-driven reporter genes. Rather, the CHIP-sequencing data for binging Nrf1 and Nrf2 obtained from the ENCODE database showed considerably weak signals on the promoters of the above-described genes (Fig. S8). This is likely owing to less amounts of the nuclearly-imported Nrf1 and Nrf2, particularly in the normal unstressed conditions or requirements of both factors for the functional heterodimerization with their putative DNA-binding partners, as well as other cofactors. As such, our further experimental evidence obtained from *Nrf1α*$^{-/-}$ cells has demonstrated that Nrf1, rather than Nrf2, can serve as a vital dominant-positive determinant of mitochondrial functioning by governing transcriptional expression of αPal^{NRF1}, GABPα^{NRF2} and PGC1α because even though hyperactive Nrf2 was accumulated, it cannot compensate for a fatal defect in basal expression of αPal^{NRF1}, GABPα^{NRF2} and PGC1α in *Nrf1α*$^{-/-}$ cells. But, no decrease of PGC1β was determined in *Nrf1α*$^{-/-}$ cells, although it was reportedly regulated by Nrf1 in mouse cells [23]; this difference may be attributable to distinct cell types in between the human and mouse species. Moreover, when cells are required for impaired mitochondrial function, a highly-conserved mechanism called UPR^{mt} is activated to trigger cell repair of the mitochondrial function. Such UPR^{mt}-related genes were still activated by FCCP-induced mitochondrial stress in *Nrf2*$^{-/-}$ cells but were almost unaffected in *Nrf1α*$^{-/-}$ cells. Thereby, it is inferable that the mitochondrial UPR^{mt} is prevented or even completely abolished in *Nrf1α*$^{-/-}$ cells, due to its fetal mitochondrial damage arising from the loss of Nrf1α's function. This finding further indicates that Nrf1, but not Nrf2, is an indispensable dominantly-determining factor in maintaining mitochondrial homeostasis and its integrity, albeit Nrf2 is also involved in this process.

4.3. *Nrf2 exerts a 'double-edged sword's role in the redox regulation, particularly in Nrf1α*$^{-/-}$ *cells*

Mitochondria produce ROS mainly from escaped electrons in the transport respiratory chain, and these electrons [e^-, together with hydrogen ion (H^+)] originated primarily from aerobic glycolysis. Herein, it is, to our surprise, found that the apparent rise and fall of the intracellular ROS levels in *Nrf1α*$^{-/-}$ cells are accompanied by an increase or decrease of glycolysis, respectively when they had been treated with its activator insulin or inhibitor 2-DG. This is also supported by additional observations showing that the yield of ROS in 5 mM-glucose cultured *Nrf1α*$^{-/-}$ cells is at a rather lower level than that arising from the 25 mM glucose cultured conditions. Similar glucose effects on the yield of ROS were also manifested in wild-type cells, but *Nrf2*$^{-/-}$ cells appeared to make little difference. Further experiments revealed that basal expression levels of glycolysis and lipid synthesis-related genes were up-regulated in *Nrf1α*$^{-/-}$ cells, but also enabled to be interfered to considerably lower extents by silencing of Nrf2. Collectively, these data suggest that hyperactive Nrf2 accumulated in *Nrf1α*$^{-/-}$ cells has a strong ability to promote glycolysis and lipid biosynthesis insomuch as to give rise to excessive ROS from its mitochondria, particularly under the pressure of a high glycolysis flow. In addition, we found that insulin can increase the expression of Nrf1, and 5 mM glucose cultured conditions (glucose restricted medium) reduce the expression of Nrf1 (Figs. S10C and S10F). When cells are treated with high concentrations of glycolysis inhibitors (2-DG) or starved in a non-glucose medium, glycosylated Nrf1 decrease and the active isoform of Nrf1 significant increase (Fig. S10G) [54]. This also implies the relevance between Nrf1 and glucose metabolism. Perhaps under lower metabolic conditions Nrf1 is down-regulated to weaken mitochondrial-related metabolism, and under extreme glucose deficiency conditions Nrf1 is transitorily activated to enhance mitochondrial function to meet the needs of energy and promote the metabolism of non-sugar substances such as lipids, but that requires more experiments to prove.

Among those genes possibly mediated by Nrf2, PDH plays a role in controlling the entry of pyruvate produced by glycolysis into mitochondria, particularly when PDH is elevated concomitantly with unchanged LDHA, in *Nrf1α*$^{-/-}$ cells, making the flue flow produced by glycolysis more easily enter the mitochondria. However, fatal damage to the electron transport chain slows down the TCA cycle [67], it is hence difficult for the impaired TCA cycle to consume acetyl-CoA that enters the mitochondria in *Nrf1α*$^{-/-}$ cells. The resulting increase in fatty acid biosynthesis provoked by hyperactive Nrf2 provides an alternative way to consume the metabolites from the increased glycolysis flow. This enables to allow the citric acid produced by oxaloacetate and acetyl-CoA to skip most of the damaged TCA cycle and then convert it into apple acids. Overall, deficiency of Nrf1α cannot only lead to a marked increase in intracellular ROS yield from its defective mitochondria, and also augment glucose consumption and lipid biosynthesis by increasing Nrf2 to aggravate ROS production. Such incremented lipid biosynthesis may be explained as a reasonable cause of lipid deposition in *Nrf1*$^{-/-}$cells, ultimately resulting in the spontaneous development of non-alcoholic steatohepatitis and ensuing hepatoma in liver-specific *Nrf1*$^{-/-}$ mice [27,29].

Notably, a direct main source of ROS arises from the electron escape of NADH produced by cellular metabolism in the respiratory chain. Such escaped electrons enable exacerbation of the mitochondrial membrane potential (Δψm) to a rather higher degree due to the increasingly sluggish electron transport within a longer half-life of relevant respiratory chain intermediates [68]. This is distinctive from destructive uncoupling, because a modest decrease in Δψm, called 'mild uncoupling', has been shown to exert a cytoprotective effect [69]. Thereby, we also found that UCP2 is negatively regulated by hyperactive Nrf2 in *Nrf1α*$^{-/-}$ cells to increase the intracellular ROS production, even though Nrf2 has been generally accepted as a master regulator of the antioxidant and detoxifying system and also as a key player in metabolic regulation. When required for cellular demands, UCP2 is widely expressed, so that it cannot only relieve the pressure of the electron transport chain and also reduce byproducts of ROS from mitochondria, but the resulting production of ATP is decreased concomitantly by reducing Δψm. Thus, it is inferable that Nrf2 is selectively allowed for inhibition of UCP2 to facilitate the energetic production of ATP, albeit with an accompanying increase in the mitochondrial ROS byproducts, particularly in *Nrf1α*$^{-/-}$ cells. Conversely, when UCP2 was over-expressed, the yield of ROS in *Nrf1α*$^{-/-}$ cells was greatly reduced, but in *Nrf2*$^{-/-}$ cells was unchanged similarly to *WT* controls, implying

that UCP2 is also selectively contributable to antioxidant cytoprotection. Further experiments unraveled that UCP2 is negatively regulated by Nrf2 through ARE-driven miR-195 and/or miR-497. The expression levels of miR-195 and miR-497 were up-regulated by hyperactive Nrf2 in *Nrf1α*$^{-/-}$ cells, even albeit both can also be regulated directly by Nrf1. In addition, Kuosmanen *et al.* identified 116 novel Nrf2-targeted miRNAs by CHIP-sequencing, including miR195 and miR497 [70], as fully consistent with our results. Altogether, these demonstrate that Nrf2 cannot only exert its intrinsic antioxidant effect but also promote the generation of ROS within proper tempo-spatial contexts. And it also indicates that Nrf2 does not only play a role in the antioxidant, but also, more importantly, regulates the balance between production of ROS and their elimination, and even another balance existing between ROS elimination and energy production, albeit this requires further investigation.

4.4. Inter-regulatory effects of Nrf1 and Nrf2 are integrated by multiple signaling to gene expression networks

Several studies have uncovered that Nrf2 acts as a versatile chameleon-like player in both cancer prevention and promotion [71], but its oncogenic activity to promote cancer development is tightly confined by Nrf1 (along with its long isoform TCF11), which is endowed as a potent tumor-repressor [26,29,30]. Such oppositely inter-regulatory effects of Nrf1 and Nrf2 are unified integrally by multiple redox signaling pathways to cognate gene expression networks at distinct levels (Fig. 8A). These multi-hierarchical signaling networks gradually converged on the base of redox regulation by Nrf1 and Nrf2 (Fig. 8B). Of note, the primary ROS-caused stress and secondary oxidative damages are well known to serve as an initiator of cancer development and also as a promotor of cancer progression and malignance [72]. However, our evidence revealed that significantly elevated ROS in *Nrf2*$^{-/-}$ cells does not render its migration ability and growth rate to be increased, but conversely becomes weaker than *WT* controls. Further xenograft animal experiments by inoculating *Nrf2*$^{-/-}$ cells unraveled that loss of Nrf2's function leads to a striking reduction *in vivo* malgrowth of hepatoma and its metastasis [29]. These indicate that loss of Nrf2-mediated antioxidant and detoxifying cytoprotection results in certain 'mild extents' of ROS that are not enough to sufficiently initiate cancer development or promote malignant progression, but conversely can serve as eustress to stimulate beneficial hormesis effects.

By contrast with *Nrf2*$^{-/-}$ cells, severe extents of ROS-caused distress and damages are determined in *Nrf1α*$^{-/-}$ cells, although accompanied by hyperactive Nrf2 accumulation and reinforced antioxidant response. Such oxidative distress is attributable primarily to *Nrf1α*$^{-/-}$-leading mitochondrial dysfunction and its UPR^{mt} failure, and secondarily to Nrf2-augmenting the yield of ROS by strengthening glycolysis (resembling the Warburg's effect) to aggravate the pressure of electron respiratory chain and also by inhibiting UCP2 to enable for electron escape from the transport respiratory chain. Consequently, loss of *Nrf1α*$^{-/-}$results in marked increases in its malgrowth, migration and metastasis, as well in the EMT process [29,73]; such increased ability was also greatly prevented by silencing of Nrf2, in addition to the restored expression of Nrf1α or TCF11 [29,30]. These indicate that Nrf2 acts as a tumor-promoter to exert its oncogenic activity, only when Nrf1α/TCF11 is disrupted, whereas the latter Nrf1α/TCF11 is likely to possess an intrinsic capability to repress initiation of cancer development. This cancer-repressing effect may also be executed by two additional 'star' tumor-repressors PTEN and p53 because both were diminished in *Nrf1α*$^{-/-}$ cells. Besides, the EMT-relevant signaling, together with the MEK-MAPKs (i.e., JNK, ERKs, p38 kinase)-AP1 (JUN + FOS) and PI3K-AKT, as well as HIF1α and NF-κB, signaling networks are constitutively activated in *Nrf1α*$^{-/-}$ cells. In addition, the redox metabolic reprogramming of *Nrf1α*$^{-/-}$ cells (owing to dysfunctional mitochondria) may be contributable to cancer development and progression [35]. Contrarily, most cell killing results from the further elevated yield of ROS after *Nrf1α*$^{-/-}$ cells were stimulated by glucose deprivation. Overall, Nrf1 acts as a potent integrator of the cellular redox regulation by multi-hierarchical signaling to gene expression networks to maintain cell homeostasis and organ integrity.

In summary, systematic examinations of distinctive roles for Nrf1 and Nrf2 in redox regulation are carried out from a holistic view in a combination of reductionist approaches. The results unveiled that Nrf1 functions as an indispensable redox-determining factor for mitochondrial homeostasis because the loss of its function leads to a potentially fatal defect in dysfunctional mitochondria to give rise to severe oxidative stress along with the failure of UPR^{mt}, and such detriment effects cannot be counteracted by hyperactive Nrf2 accumulated in *Nrf1α*$^{-/-}$ cells, but conversely malgrowth of *Nrf1α*$^{-/-}$-derived tumor appears to be protected by Nrf2-strengthening antioxidant response and glycolysis pathways. From this, it is inferable that Nrf2 plays a critical role in Warburg's effect in *Nrf1α*$^{-/-}$ cells. The reinforced glycolysis aggravates the mitochondrial pressure to allow for the electron escape to yield excessive ROS, particularly when UCP2 is suppressed by hyperactive Nrf2. Therefore, the versatile Nrf2 exerts a 'double-edged sword's role in redox regulation, particularly in *Nrf1α*$^{-/-}$ cells. Such inter-regulatory effects of Nrf1 and Nrf2 are integrated by multi-hierarchical signaling towards gene expression networks to perpetuate cell homeostasis and organ integrity during development and growth.

Author contributions

S.H. performed most of the experiments except indicated elsewhere, made all figures, and wrote the manuscript draft. J.F. constructed relevant plasmids used in this study. M.W. performed a statistical analysis of transcriptome data. R.W. and K.L. participated in the detection of intracellular ROS and transmission electron microscopy. Z.Z. participated in drawing some pictures and edited the manuscript draft in English. Y.Z. designed and supervised this study, analyzed all the data, helped to prepare all figures with cartoons, and wrote and revised the paper.

Declaration of competing interest

The authors declare no conflict of interest. Besides, it should be noted that the preprinted version of this paper had been initially posted at doi: https://doi.org/10.1101/2022.05.04.490622.

Data availability

No data was used for the research described in the article.

Acknowledgments

We are greatly thankful to Dr. Yonggang Ren (North Sichuan Medical College, Sichuan, China), and Lu Qiu (Zhengzhou University, Henan, China) for their involvement in establishing the indicated cell lines used in this study. We also thank other members of Prof. Zhang's laboratory (at Chongqing University, China) for giving their invaluable help with this work. Notably, this study was funded by the National Natural Science Foundation of China (NSFC, with a key program 91429305 and additional two projects 81872336 and 82073079) awarded to Prof. Yiguo Zhang. In addition, this was in part supported by the Initiative Foundation of Jiangjin Hospital affiliated to Chongqing University (2022qdjfxm001).

Appendix A. Supplementary data

Supplementary data to this article can be found online at https://doi.org/10.1016/j.redox.2022.102470.

References

[1] H. Kong, N.S. Chandel, Regulation of redox balance in cancer and T cells, J. Biol. Chem. 293 (2018) 7499–7507.
[2] D.E. Handy, J. Loscalzo, Redox regulation of mitochondrial function, Antioxidants Redox Signal. 16 (2012) 1323–1367.
[3] K.M. Holmstrom, T. Finkel, Cellular mechanisms and physiological consequences of redox-dependent signalling, Nat. Rev. Mol. Cell Biol. 15 (2014) 411–421.
[4] H. Sies, Hydrogen peroxide as a central redox signaling molecule in physiological oxidative stress: oxidative eustress, Redox Biol. 11 (2017) 613–619.
[5] H. Sies, Oxidative eustress: on constant alert for redox homeostasis, Redox Biol. 41 (2021), 101867.
[6] J. Yuan, S. Zhang, Y. Zhang, Nrf1 is paved as a new strategic avenue to prevent and treat cancer, neurodegenerative and other diseases, Toxicol. Appl. Pharmacol. 360 (2018) 273–283.
[7] S. Yang, G. Lian, ROS and diseases: role in metabolism and energy supply, Mol. Cell. Biochem. 467 (2020) 1–12.
[8] M. Yamamoto, T.W. Kensler, H. Motohashi, The KEAP1-NRF2 system: a thiol-based sensor-effector apparatus for maintaining redox homeostasis, Physiol. Rev. 98 (2018) 1169–1203.
[9] Y. Zhang, Y. Xiang, Molecular and cellular basis for the unique functioning of Nrf1, an indispensable transcription factor for maintaining cell homoeostasis and organ integrity, Biochem. J. 473 (2016) 961–1000.
[10] Y. Xiang, M. Wang, S. Hu, L. Qiu, F. Yang, Z. Zhang, S. Yu, J. Pi, Y. Zhang, Mechanisms controlling the multistage post-translational processing of endogenous Nrf1alpha/TCF11 proteins to yield distinct isoforms within the coupled positive and negative feedback circuits, Toxicol. Appl. Pharmacol. 360 (2018) 212–235.
[11] Y. Zhang, S. Li, Y. Xiang, L. Qiu, H. Zhao, J.D. Hayes, The selective post-translational processing of transcription factor Nrf1 yields distinct isoforms that dictate its ability to differentially regulate gene expression, Sci. Rep. 5 (2015).
[12] I. Bellezza, I. Giambanco, A. Minelli, R. Donato, Nrf2-Keap1 signaling in oxidative and reductive stress, Biochim. Biophys. Acta Mol. Cell Res. 1865 (2018) 721–733.
[13] S.C. Lu, Glutathione synthesis, Biochim. Biophys. Acta 1830 (2013) 3143–3153.
[14] D.V. Chartoumpekis, N. Wakabayashi, T.W. Kensler, Keap1/Nrf2 pathway in the frontiers of cancer and non-cancer cell metabolism, Biochem. Soc. Trans. 43 (2015) 639–644.
[15] P. Nioi, J.D. Hayes, Contribution of NAD(P)H:quinone oxidoreductase 1 to protection against carcinogenesis, and regulation of its gene by the Nrf2 basic-region leucine zipper and the arylhydrocarbon receptor basic helix-loop-helix transcription factors, Mutat. Res. 555 (2004) 149–171.
[16] R. Gozzelino, V. Jeney, M.P. Soares, Mechanisms of cell protection by heme oxygenase-1, Annu. Rev. Pharmacol. Toxicol. 50 (2010) 323–354.
[17] S. Ren, Y. Bian, Y. Hou, Z. Wang, Z. Zuo, Z. Liu, Y. Teng, J. Fu, H. Wang, Y. Xu, Q. Zhang, Y. Chen, J. Pi, The roles of NFE2L1 in adipocytes: structural and mechanistic insight from cell and mouse models, Redox Biol. 44 (2021), 102015.
[18] P. Xue, Y. Hou, Z. Zuo, Z. Wang, S. Ren, J. Dong, J. Fu, H. Wang, M.E. Andersen, Q. Zhang, Y. Xu, J. Pi, Long isoforms of NRF1 negatively regulate adipogenesis via suppression of PPARgamma expression, Redox Biol. 30 (2020), 101414.
[19] S.B. Widenmaier, N.A. Snyder, T.B. Nguyen, A. Arduini, G.Y. Lee, A.P. Arruda, J. Saksi, A. Bartelt, G.S. Hotamisligil, NRF1 is an ER membrane sensor that is central to cholesterol homeostasis, Cell 171 (2017) 1094–1109, e1015.
[20] H. Zheng, J. Fu, P. Xue, R. Zhao, J. Dong, D. Liu, M. Yamamoto, Q. Tong, W. Teng, W. Qu, Q. Zhang, M.E. Andersen, J. Pi, CNC-bZIP protein Nrf1-dependent regulation of glucose-stimulated insulin secretion, Antioxidants Redox Signal. 22 (2015) 819–831.
[21] Y. Zhang, J. Nicholatos, J.R. Dreier, S.J. Ricoult, S.B. Widenmaier, G. S. Hotamisligil, D.J. Kwiatkowski, B.D. Manning, Coordinated regulation of protein synthesis and degradation by mTORC1, Nature 513 (2014) 440–443.
[22] Y. Hirotsu, C. Higashi, T. Fukutomi, F. Katsuoka, T. Tsujita, Y. Yagishita, Y. Matsuyama, H. Motohashi, A. Uruno, M. Yamamoto, Transcription factor NF-E2-related factor 1 impairs glucose metabolism in mice, Gene Cell. 19 (2014) 650–665.
[23] Y. Hirotsu, N. Hataya, F. Katsuoka, M. Yamamoto, NF-E2-related factor 1 (Nrf1) serves as a novel regulator of hepatic lipid metabolism through regulation of the Lipin1 and PGC-1beta genes, Mol. Cell Biol. 32 (2012) 2760–2770.
[24] D. Peng, A. Zaika, J. Que, W. El-Rifai, The antioxidant response in Barrett's tumorigenesis: a double-edged sword, Redox Biol. 41 (2021), 101894.
[25] M. Rojo de la Vega, E. Chapman, D.D. Zhang, NRF2 and the hallmarks of cancer, Cancer Cell 34 (2018) 21–43.
[26] Y. Ren, L. Qiu, F. Lu, X. Ru, S. Li, Y. Xiang, S. Yu, Y. Zhang, TALENs-directed knockout of the full-length transcription factor Nrf1alpha that represses malignant behaviour of human hepatocellular carcinoma (HepG2) cells, Sci. Rep. 6 (2016), 23775.
[27] Z. Xu, L. Chen, L. Leung, T.S. Yen, C. Lee, J.Y. Chan, Liver-specific inactivation of the Nrf1 gene in adult mouse leads to nonalcoholic steatohepatitis and hepatic neoplasia, Proc. Natl. Acad. Sci. U.S.A. 102 (2005) 4120–4125.
[28] T. Tsujita, V. Peirce, L. Baird, Y. Matsuyama, M. Takaku, S.V. Walsh, J.L. Griffin, A. Uruno, M. Yamamoto, J.D. Hayes, Transcription factor Nrf1 negatively regulates the cystine/glutamate transporter and lipid-metabolizing enzymes, Mol. Cell Biol. 34 (2014) 3800–3816.
[29] L. Qiu, M. Wang, S. Hu, X. Ru, Y. Ren, Z. Zhang, S. Yu, Y. Zhang, Oncogenic activation of Nrf2, though as a master antioxidant transcription factor, liberated by specific knockout of the full-length Nrf1alpha that acts as a dominant tumor repressor, Cancers 10 (2018).
[30] M. Wang, Y. Ren, S. Hu, K. Liu, L. Qiu, Y. Zhang, TCF11 has a potent tumor-repressing effect than its prototypic Nrf1alpha by definition of both similar yet different regulatory profiles, with a striking disparity from Nrf2, Front. Oncol. 11 (2021), 707032.
[31] L. Leung, M. Kwong, S. Hou, C. Lee, J.Y. Chan, Deficiency of the Nrf1 and Nrf2 transcription factors results in early embryonic lethality and severe oxidative stress, J. Biol. Chem. 278 (2003) 48021–48029.
[32] S.N. Zucker, E.E. Fink, A. Bagati, S. Mannava, A. Bianchi-Smiraglia, P.N. Bogner, J. A. Wawrzyniak, C. Foley, K.I. Leonova, M.J. Grimm, K. Moparthy, Y. Ionov, J. Wang, S. Liu, S. Sexton, E.S. Kandel, A.V. Bakin, Y. Zhang, N. Kaminski, B. H. Segal, M.A. Nikiforov, Nrf2 amplifies oxidative stress via induction of Klf9, Mol. Cell. 53 (2014) 916–928.
[33] A. Bansal, M.C. Simon, Glutathione metabolism in cancer progression and treatment resistance, J. Cell Biol. 217 (2018) 2291–2298.
[34] A.V. Budanov, J.H. Lee, M. Karin, Stressin' Sestrins take an aging fight, EMBO Mol. Med. 2 (2010) 388–400.
[35] Y.P. Zhu, Z. Zheng, Y. Xiang, Y. Zhang, Glucose starvation-induced rapid death of nrf1alpha-deficient, but not nrf2-deficient, hepatoma cells results from its fatal defects in the redox metabolism reprogramming, Oxid. Med. Cell. Longev. 2020 (2020), 4959821.
[36] N. Li, K. Ragheb, G. Lawler, J. Sturgis, B. Rajwa, J.A. Melendez, J.P. Robinson, Mitochondrial complex I inhibitor rotenone induces apoptosis through enhancing mitochondrial reactive oxygen species production, J. Biol. Chem. 278 (2003) 8516–8525.
[37] R.J. Youle, A.M. van der Bliek, Mitochondrial fission, fusion, and stress, Science 337 (2012) 1062–1065.
[38] S. Zhang, Y. Deng, Y. Xiang, S. Hu, L. Qiu, Y. Zhang, Synergism and antagonism of two distinct, but confused, Nrf1 factors in integral regulation of the nuclear-to-mitochondrial respiratory and antioxidant transcription networks, Oxid. Med. Cell. Longev. 2020 (2020), 5097109.
[39] Y.P. Zhu, Y. Xiang, A. L'Honore, D. Montarras, M. Buckingham, Y. Zhang, Commentary on distinct, but previously confused, Nrf1 transcription factors and their functions in redox regulation, Dev. Cell 53 (2020) 377–378.
[40] W. Di, J. Lv, S. Jiang, C. Lu, Z. Yang, Z. Ma, W. Hu, Y. Yang, B. Xu, PGC-1: the energetic regulator in cardiac metabolism, Curr. Issues Mol. Biol. 28 (2018) 29–46.
[41] R. Wufuer, Z. Fan, K. Liu, Y. Zhang, Differential yet integral contributions of Nrf1 and Nrf2 in the human HepG2 cells on antioxidant cytoprotective response against tert-butylhydroquinone as a pro-oxidative stressor, Antioxidants 10 (2021).
[42] G.S. Shadel, T.L. Horvath, Mitochondrial ROS signaling in organismal homeostasis, Cell 163 (2015) 560–569.
[43] L. Qiu, Q. Yang, W. Zhao, Y. Xing, P. Li, X. Zhou, H. Ning, R. Shi, S. Gou, Y. Chen, W. Zhai, Y. Wu, G. Li, Z. Chen, Y. Ren, Y. Gao, Y. Zhang, Y. Qi, Dysfunction of the energy sensor NFE2L1 triggers uncontrollable AMPK signaling and glucose metabolism reprogramming, Cell Death Dis. 13 (2022) 501.
[44] G.A. Breen, I.E. Scheffler, Respiration-deficient Chinese hamster cell mutants: biochemical characterization, Somat. Cell Genet. 5 (1979) 441–451.
[45] G. Baffy, Uncoupling protein-2 and cancer, Mitochondrion 10 (2010) 243–252.
[46] A. Bartelt, S.B. Widenmaier, C. Schlein, K. Johann, R.L.S. Goncalves, K. Eguchi, A. W. Fischer, G. Parlakgul, N.A. Snyder, T.B. Nguyen, O.T. Bruns, D. Franke, M. G. Bawendi, M.D. Lynes, L.O. Leiria, Y.H. Tseng, K.E. Inouye, A.P. Arruda, G. S. Hotamisligil, Brown adipose tissue thermogenic adaptation requires Nrf1-mediated proteasomal activity, Nat. Med. 24 (2018) 292–303.
[47] B.D. Fink, Y.S. Hong, M.M. Mathahs, T.D. Scholz, J.S. Dillon, W.I. Sivitz, UCP2-dependent proton leak in isolated mammalian mitochondria, J. Biol. Chem. 277 (2002) 3918–3925.
[48] T. Shpilka, C.M. Haynes, The mitochondrial UPR: mechanisms, physiological functions and implications in ageing, Nat. Rev. Mol. Cell Biol. 19 (2018) 109–120.
[49] L. Li, Y. Chen, C. Chenzhao, S. Fu, Q. Xu, J. Zhao, Glucose negatively affects Nrf2/SKN-1-mediated innate immunity in C. elegans, Aging 10 (2018) 3089–3103.
[50] C.M. Haynes, Y. Yang, S.P. Blais, T.A. Neubert, D. Ron, The matrix peptide exporter HAF-1 signals a mitochondrial UPR by activating the transcription factor ZC376.7 in C. elegans, Mol. Cell 37 (2010) 529–540.
[51] C.J. Fiorese, A.M. Schulz, Y.F. Lin, N. Rosin, M.W. Pellegrino, C.M. Haynes, The transcription factor ATF5 mediates a mammalian mitochondrial UPR, Curr. Biol. : CB 26 (2016) 2037–2043.
[52] S. Michel, M. Canonne, T. Arnould, P. Renard, Inhibition of mitochondrial genome expression triggers the activation of CHOP-10 by a cell signaling dependent on the integrated stress response but not the mitochondrial unfolded protein response, Mitochondrion 21 (2015) 58–68.
[53] P.M. Quiros, M.A. Prado, N. Zamboni, D. D'Amico, R.W. Williams, D. Finley, S. P. Gygi, J. Auwerx, Multi-omics analysis identifies ATF4 as a key regulator of the mitochondrial stress response in mammals, J. Cell Biol. 216 (2017) 2027–2045.
[54] Y.P. Zhu, Z. Zheng, S. Hu, X. Ru, Z. Fan, L. Qiu, Y. Zhang, Unification of opposites between two antioxidant transcription factors Nrf1 and Nrf2 in mediating distinct cellular responses to the endoplasmic reticulum stressor tunicamycin, Antioxidants 9 (2019).
[55] M.E. Fusakio, J.A. Willy, Y. Wang, E.T. Mirek, R.J. Al Baghdadi, C.M. Adams, T. G. Anthony, R.C. Wek, Transcription factor ATF4 directs basal and stress-induced gene expression in the unfolded protein response and cholesterol metabolism in the liver, Mol. Biol. Cell 27 (2016) 1536–1551.
[56] B.P. Tremblay, C.M. Haynes, Mitochondrial distress call moves to the cytosol to trigger a response to stress, Nature 579 (2020) 348–349.
[57] E. Fessler, E.M. Eckl, S. Schmitt, I.A. Mancilla, M.F. Meyer-Bender, M. Hanf, J. Philippou-Massier, S. Krebs, H. Zischka, L.T. Jae, A pathway coordinated by DELE1 relays mitochondrial stress to the cytosol, Nature 579 (2020) 433–437.
[58] B.J. Berry, T.O. Nieves, A.P. Wojtovich, Decreased mitochondrial membrane potential activates the mitochondrial unfolded protein response, MicroPubl. Biol 2021 (2021).

[59] A. Barrallo-Gimeno, M.A. Nieto, The Snail genes as inducers of cell movement and survival: implications in development and cancer, Development 132 (2005) 3151–3161.
[60] E.F. Wagner, A.R. Nebreda, Signal integration by JNK and p38 MAPK pathways in cancer development, Nat. Rev. Cancer 9 (2009) 537–549.
[61] J.N. Moloney, T.G. Cotter, ROS signalling in the biology of cancer, Semin. Cell Dev. Biol. 80 (2018) 50–64.
[62] Y. Mitsuishi, K. Taguchi, Y. Kawatani, T. Shibata, T. Nukiwa, H. Aburatani, M. Yamamoto, H. Motohashi, Nrf2 redirects glucose and glutamine into anabolic pathways in metabolic reprogramming, Cancer Cell 22 (2012) 66–79.
[63] Y. Zhou, S. Duan, Y. Zhou, S. Yu, J. Wu, X. Wu, J. Zhao, Y. Zhao, Sulfiredoxin-1 attenuates oxidative stress via Nrf2/ARE pathway and 2-Cys Prdxs after oxygen-glucose deprivation in astrocytes, J. Mol. Neurosci. : MN 55 (2015) 941–950.
[64] Y.K. Lee, H.G. Woo, G. Yoon, Mitochondrial defect-responsive gene signature in liver-cancer progression, BMB reports 48 (2015) 597–598.
[65] Y.K. Lee, S.M. Kwon, E.B. Lee, G.H. Kim, S. Min, S.M. Hong, H.J. Wang, D.M. Lee, K.S. Choi, T.J. Park, G. Yoon, Mitochondrial respiratory defect enhances hepatoma cell invasiveness via STAT3/NFE2L1/STX12 Axis, Cancers 12 (2020).
[66] C. Kukat, N.G. Larsson, mtDNA makes a U-turn for the mitochondrial nucleoid, Trends Cell Biol. 23 (2013) 457–463.
[67] M. Donnelly, I.E. Scheffler, Energy metabolism in respiration-deficient and wild type Chinese hamster fibroblasts in culture, J. Cell. Physiol. 89 (1976) 39–51.
[68] M.D. Brand, C. Affourtit, T.C. Esteves, K. Green, A.J. Lambert, S. Miwa, J.L. Pakay, N. Parker, Mitochondrial superoxide: production, biological effects, and activation of uncoupling proteins, Free Radic. Biol. Med. 37 (2004) 755–767.
[69] A.A. Starkov, Mild" uncoupling of mitochondria, Biosci. Rep. 17 (1997) 273–279.
[70] S. Linna-Kuosmanen, V. Tomas Bosch, P.R. Moreau, M. Bouvy-Liivrand, H. Niskanen, E. Kansanen, A. Kivela, J. Hartikainen, M. Hippelainen, H. Kokki, P. Tavi, A.L. Levonen, M.U. Kaikkonen, NRF2 is a key regulator of endothelial microRNA expression under proatherogenic stimuli, Cardiovasc. Res. 117 (2021) 1339–1357.
[71] M. Rojo de la Vega, E. Chapman, D.D. Zhang, NRF2 and the Hallmarks of Cancer, Cancer Cell, 2018.
[72] J.D. Hayes, A.T. Dinkova-Kostova, K.D. Tew, Oxidative stress in cancer, Cancer Cell 38 (2020) 167–197.
[73] Y. Ren, L. Qiu, F. Lü, X. Ru, S. Li, Y. Xiang, S. Yu, Y. Zhang, TALENs-directed knockout of the full-length transcription factor Nrf1a that represses malignant behaviour of human hepatocellular carcinoma (HepG2) cells, Sci. Rep. 7 (2016). Accepted for publication.